Journal of Energy Storage 168 (2026) 122559

Contents lists available at ScienceDirect

Journal of Energy Storage

journal homepage: www.elsevier.com/locate/est

Research papers

Long cycle and calendar life of Si-based Li-ion batteries enabled by localized high-concentration electrolytes and their surprising water tolerance

Lydia Meyer [a,*], Marco-T.F. Rodrigues [b], Kevin Gering [c], Danielle Henckel [a], Andrew Dopilka [d], Nessa Majaya [e], Robert Kostecki [d], Kristin Persson [e], Gabriel M. Veith [f,g], Andrew M. Colclasure [a], Maxwell C. Schulze [a]

[a] National Laboratory of the Rockies, Golden, CO, United States
[b] Argonne National Laboratory, Lemont, IL, United States
[c] Idaho National Laboratory, Idaho Falls, ID, United States
[d] Lawrence Berkeley National Laboratory, Berkeley, CA, United States
[e] University of California, Berkeley, Berkeley, CA, United States
[f] Oak Ridge National Laboratory, Oak Ridge, TN, United States
[g] University of Tennessee, Knoxville, TN, United States

ARTICLE INFO

Keywords:
Localized high concentration electrolytes
Silicon anodes
Electrolytes
Solid electrolyte interphase
Calendar aging
Li-ion batteries

ABSTRACT

Silicon-based anodes promise an increase in energy density for Li-ion batteries, yet they suffer from a poor calendar life. Researchers have posited that fluorinated lithium salt forms reactive side products that destroy the solid electrolyte interphase (SEI), even without cycling. HF is one such reactive side product formed from trace water contamination in the electrolyte. Some electrolytes, such as localized high concentration electrolytes (LHCEs) may improve cell stability in highly reactive systems, such as Li metal and Si. In the present study, LHCEs containing 200–300 ppm of water retained up to 8% greater capacity (1200–1300 mAh/g Si) in calendar life tests over 200 days compared to dried electrolytes (< 20 ppm water). Calendar aging took place at 100% state of charge. Cells with 200–300 ppm water performed comparably to cells with 20 ppm water in cycle life tests (900–1000 mAh/g Si) . Even adding 1000 ppm water did not lead to rapid capacity fade in cells undergoing cycle life tests. Nano-FTIR spectroscopy revealed chemical and structural differences in the SEI for cells with 1000 ppm water compared to 200–300 ppm water. The SEI differences, including increased Li_2O concentration, may have contributed to improved calendar life. This research reveals the capabilities of LHCEs to improve the calendar and cycle life of Si-based Li-ion batteries, despite the presence of a highly reactive contaminant.

1. Introduction

Silicon-based anodes promise greatly increased specific capacity compared to traditional graphite anodes, but they suffer from increased reactivity and capacity fade [1–5]. Although researchers have identified several interrelated causes of capacity fade, solid electrolyte interphase (SEI) dissolution due to HF formation of the electrolyte has been hypothesized as a degradation mechanism by the U.S Department of Energy Silicon Consortium Project [6,7]. Specifically, the PF_6^- anion of the $LiPF_6$ salt reacts with small amounts of water in the electrolyte to form HF, which could degrade the SEI and cause etching of the silicon active material [7–10]. Generally, $LiPF_6$ and water have long been associated with SEI degradation and cell capacity fade outside of Si-based cells [11–15]. Additionally, commercial Li-ion battery manufacturing requires a dry room for cell assembly and electrolyte filling [16].

$LiPF_6$ has been a standard choice of lithium salt for its low cost, effective transport properties in carbonate-based solvents, thermal stability, its passivation of aluminum at high potentials, and its ability to form a highly fluorinated SEI, which may contribute to SEI durability and anode passivation [17–24]. Some research indicates that not all water $LiPF_6$ interactions harm cell performance. Researchers from Dalhousie University intentionally doped water into electrolytes with $LiPF_6$ and showed improvements in performance metrics for cells with both graphite and lithium titanate oxide (LTO) anodes [25,26]. They found that adding even 1000 ppm of water to graphite/lithium cobalt oxide (LCO) cells did not harm pouch cell performance by considering several metrics, including charge transfer resistance, voltage drop, Coulombic efficiency, and charge slippage. They did, however, observe significantly more gassing in cells with high water concentrations, though the

* Corresponding author.
E-mail address: Lydia.Meyer@nlr.gov (L. Meyer).

https://doi.org/10.1016/j.est.2026.122559
Received 16 January 2026; Received in revised form 14 April 2026; Accepted 2 May 2026
Available online 12 May 2026

gassing did not appear to be related to cell performance. Some studies also indicate that high water concentrations (up to 2000 ppm) in the cell did not harm cell performance, even when combined with $LiPF_6$ salt [27,28]. Cells with other lithium salts also remain unaffected by water in the electrolyte [12,29]. Another common salt, Li bis(fluorosulfonyl)imide (LiFSI) can still undergo a hydrolysis reaction at elevated temperatures; however, hydrolysis has not been reported in a battery system under normal operating conditions [30].

These results indicate that the relationship between water, $LiPF_6$, and SEI is potentially more complex than previously understood [31,32]. The SEI chemical composition on a graphite anode and a Si-based anode, given the same electrolyte and formation protocol, contain many similar species, so an intrinsic chemical incompatibility with $LiPF_6$, water, and a Si-based SEI is unlikely [33–38]. Water has been associated with the formation of harmful hydrogen gas, though there is debate in the literature whether it is the primary source of hydrogen gas [39]. Water can also function both as a proton source and an oxygen donor, which could be highly detrimental or advantageous, respectively. Protons in battery electrolyte have been found to cause cathode-electrolyte interface (CEI) destruction, and H^+ can also participate in unwanted side reactions [40]. Oxygen donation from water may result in the formation of Li_2O as an SEI product. While teasing apart the relative contributions of any one SEI product is non-trivial, Li_2O has been associated with improved performance in both liquid- and solid-state systems [41–43].

Although removing water from the electrolyte components is feasible, it can be costly and time-consuming. Researchers remove water from electrolyte salts and solvents with many different techniques, including drying under vacuum, molecular sieves, activated alumina, etc. [44–46] These techniques may require specialized equipment, additional mixing and filtration steps, and several days of downtime as drying occurs. Researchers also add water scavenging additives and separator materials, though utilizing these materials may require long-term study to determine performance and lifetime impacts and could increase the cost of the cell [47–50].

While limiting water in the electrolyte could eliminate some cell health concerns, choosing a less reactive electrolyte may be a better solution. Recent electrolyte research has targeted localized high concentration (LHCEs) for improved stability against more reactive electrodes. The design principle of LHCEs is to exploit the benefits of a highly concentrated electrolyte (HCE), while retaining some properties of a dilute carbonate-based electrolyte [51]. The advantages of an HCE include a thin, anion-derived SEI that is durable over the course of many cycles. This is because the highly concentrated salt/solvent mixture yields solvation structures, including contact ion pairs (CIPs) and aggregates (AGGs), that include the anion in the solvation shell of Li-ions in higher proportions, compared to a dilute electrolyte. Instead of solvating lithium distantly, the anion participates more readily in solvation and thus SEI formation. The anion derived SEI has been associated with long-duration cycling stability [51–53]. The increased lithium salt concentration in an HCE, however, adds considerable cost, viscosity, and density. The LHCE is made by adding a non-participating solvent, a diluent, to the HCE. This improves the transport and other physical properties of the electrolyte while retaining HCE benefits for SEI [54–58].

LHCEs have shown significant improvements over more traditional electrolytes, particularly in Li-metal batteries [59–64]. The use of LHCEs in Li-metal battery chemistry has resulted in more stable cycling performance, improved battery lifetime, and an anion-derived SEI. Researchers have shown that the anion-derived SEI is more stable against the highly reactive Li metal anode and other anode materials [65–67]. While many forms of Si-based anodes utilize polymer and/or carbon coatings that should improve surface passivation, Si-based anodes still have a highly reactive active material versus electrolyte at high potentials, compared to more common anodes like graphite or LTO [68,69]. Furthermore, the large volume expansion and contraction of Si-based anodes likely results in continuous new exposure of reactive Si surfaces to electrolyte regardless of initial coating quality [70,71]. Si-based batteries with LHCEs have exhibited improved performance in terms of interphase stability [72] and capacity retention during calendar aging, though the exact mechanisms are not well understood [73].

Recent studies showing improvement of Si anode calendar life utilize LHCEs containing LiFSI, rather than $LiPF_6$ [72,73]. Previous research hypothesized $LiPF_6$ hydrolysis as the underlying calendar aging mechanism [6,7]. While LiFSI has not been reported to undergo hydrolysis in a battery, it can hydrolyze under specific conditions, but the literature on this topic contains competing findings [30,74,75]. The causal linkage between Si-based anode calendar life, electrolyte formulation, and contaminants has not been strongly established. Continued development of LHCEs for Si-based anodes necessitates further investigation into what exactly improves performance. The most clear distinction based on the literature is different effects of contaminants across electrolyte systems.

In this research, Si-based batteries containing two different LHCEs demonstrated high capacity retention in both calendar and cycle life testing. Cells containing LHCEs with moderate water concentration even showed improved capacity in calendar life testing over cells with low water concentrations. Water also had limited deleterious effects on cycle life, even up to 1000 ppm in some cases. Three causal mechanisms were investigated: (1) electrolyte oxidation temporarily increasing capacity before causing ultimate cell failure, (2) beneficial effects on SEI chemistry, and (3) advantageous coordination environment changes. This research highlights the importance of mechanistic investigation into novel electrolyte chemistries and contaminants for Si-based battery development.

2. Methods

2.1. Electrolyte preparation

Electrolytes with three different amounts of water were prepared for this study, < 20 ppm (low concentration), ≈ 200-300 ppm (moderate concentration), and 1000 ppm (high concentration). Electrolytes with 200-300 ppm water were made using salt and solvents without any drying procedures. The water concentrations of the solvents were measured using Karl Fischer titration. The solvents and respective water concentrations used in this study include 1,1,2,2-tetrafluoro-3-(1,1,2,2-tetrafluoroethoxy)propane (TTE) (Synquest Laboratories, battery grade, 269 ppm), 1,2-dimethoxyethane (DME) (Sigma Aldrich, anhydrous, 29 ppm), and sulfolane (TMS) (Sigma Aldrich, 98%, 333 ppm). Solvents were dried over activated alumina (Thermo Scientific) for five days. The activated alumina was dried previously in a vacuum oven at 200 °C for three days. The activated alumina was filtered out of the solvent using syringe filters (0.45 μm, Fisher Scientific). The Li salt used in this research was lithium bis(fluorosulfonyl)imide (LiFSI) (Solvionic). The LiFSI was dried under vacuum for three days in an oven internal to an argon-filled glovebox at 80 °C. The electrolytes with 1000 ppm water were formulated by first mixing the as received solvents and salt, then removing the solution from the glovebox. The weight of the electrolyte was measured and 0.1% water by mass was added to the electrolyte. The electrolyte was then replaced inside the glovebox for coin cell building.

The electrolytes studied in this research were prepared using molar ratios [76] of lithium salt and solvent components. The electrolytes studied include 1 (mole) LiFSI/1.2 DME/3 TTE and 1 LiFSI/3 TMS/3 TTE. All electrolytes were prepared in an argon-filled glovebox. The DME-based electrolyte was prepared by first adding 1.2 mole equivalents of DME to one mole equivalent of LiFSI and stirring for 30 min or until the LiFSI was dissolved. Then, three mole equivalents of TTE were added to the DME/TTE mixutre, and the solution was mixed for another 30 min. The TMS-based electrolyte was prepared by first melting the TMS at 70 °C for 20 min. One mole equivalent of LiFSI was mixed with

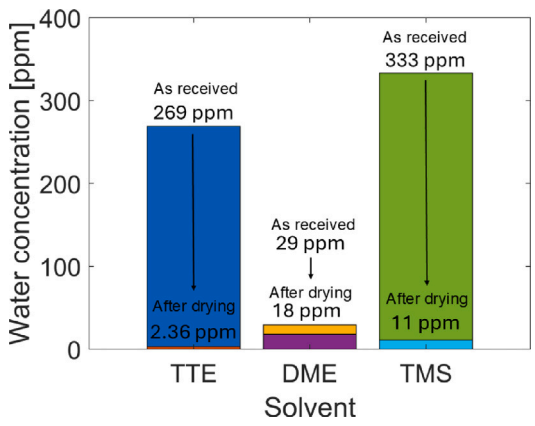

Fig. 1. Water concentrations of electrolyte solvents were measured before and after drying over activated alumina.

three mole equivalents of TMS. The LiFSI/TMS mixture was stirred at 70 °C for 30 min or until the LiFSI was completely dissolved. Three mole equivalents of TTE were then added to the LiFSI/TMS mixture, and the solution was stirred at ambient temperature for 30 min.

2.2. Karl Fischer titration

The water concentration of the solvents was measured using a Karl Fischer titrator (Mettler Toledo) and Hydranal NEXTGEN Coulomat (Honeywell) inside an argon-filled glovebox. The measurements were completed in triplicate before and after drying over activated alumina. The triplcate measurements were averaged for each solvent. Fig. 1 shows water concentrations measured before and after solvent drying. Karl Fischer titration was conducted for both the individual reagents (DME, TMS, TTE) and the electrolytes (DME- and TMS-based). The concentration of water in the LiFSI salt was calculated according to the equation

$$C_k = \frac{C_{total} \cdot \sum_i (n_i M_i) - \sum_{i \neq k} n_i M_i C_i}{n_k M_k} \quad (1)$$

where C_k is the water concentration in the LiFSI salt, C_{total} is the water concentration in the electrolyte, n is the number of moles of each component, and M is the molar mass of each component. For the TMS-based electrolyte, this resulted in a LiFSI water concentration of 17 ppm. For the DME-based electrolyte, the LiFSI water concentration was 30 ppm. The discrepancy could be due to (1) measurement-to-measurement differences or (2) differences in reactivity between the two electrolytes. Initial measurements of the water standard (Supelco Aquastar 0.01%), used for instrument calibration, varied up to 20 ppm between measurements, so the accuracy within 20 ppm may be limited. Alternatively, the TMS-based electrolyte may be more reactive, so some of the initial water contribution from the LiFSI salt may have reacted and formed a different product. Because of the small relative contribution of water to the electrolyte, water concentrations of the electrolyte are based primarily on the solvent water concentrations: ≈200 ppm for the DME-based electrolyte and ≈250 ppm for the TMS-based electrolyte.

2.3. Coin cells for calendar life measurements

Coin cells were prepared to test the calendar life of cells with both low and moderate water concentrations in LHCEs. Cells were fabricated in duplicate for electrolytes with low water concentration and in quadruplicate for electrolytes with moderate water concentration. The 2032 coin cells for calendar life testing were fabricated in an argon-filled glovebox with stainless steel hardware (UMC Corp). The anodes were manufactured with silicon synthesized in a plasma-enhanced chemical vapor deposition process (PECVD) using a non-thermal RF-enhanced plasma reactor. This manufacturing process has been described in previous research [36,77–79]. The anode (d=14 mm) was polyethylene oxide (PEO) coated Si nanoparticles (d=6 nm) with a copper current collector (t=15 μm). The PEO coating aids in processing the Si nanoparticles into a slurry for electrode coating, but the electrodes are annealed at 550 °C, so the PEO decomposes prior to cell fabrication [77]. The anode was coated with a wet gap of 50 μm and had a capacity of about 1 mAh cm^{-2}. The anodes were coated by hand, which resulted in some heterogeneity in mass loading between electrode punches. The separator used in the cells was Celgard 2325 (d=19 mm).

For calendar life testing, the cathode was lithium iron phosphate (LFP) (1.88 mAh cm^{-2}) made by the Cell Analysis, Modeling, and Prototyping (CAMP) facility at Argonne National Laboratory. The negative-to-positive (N/P) capacity ratio was approximately 0.53. This N/P ratio was used to compensate for large irreversible losses of lithium when using non-prelithiated Si anodes. During formation cycling, a significant portion of the cathode Li supply is lost to SEI formation. With a more typical N/P ratio (1–1.2), the cathode would be Li deficient, and it would be difficult to isolate the performance of the Si anode itself. Previous investigation by Rodrigues showed that a Li reservoir in a Si-based anode resulted in misrepresentation of aging due to loss of lithium inventory (LLI) [80]. Because the lithium inventory remains in excess after formation in the cells used in this study, capacity fade in these cells only represents loss of active material (LAM).

The cells were filled with 40 μL of electrolyte and rested for four hours after assembly. The volume-to-pore (V/p) ratio for these cells is difficult to pinpoint because the nanostructure of the silicon likely makes the pores very small. The V/p ratio was likely between 6–7. The cells were cycled in a temperature controlled chamber (Maccor). The cells were formed over three C/10 cycles (2.7–3.44), a 48-hour voltage hold at 3.44 V, and 10 C/3 cycles at 45 °C. The higher temperature was used in the calendar aging to intentionally accelerate all types of aging modes, including potential salt hydrolysis so that the performance of the different LHCEs and water contents could be sufficiently distinguished in a shorter time. The cells underwent a protocol that repeats open-circuit-voltage (OCV) calendar aging in between reference performance tests (RPTs). This calendar aging protocol is an adaption of a calendar aging United States Advanced Battery Consortium (USABC) protocol [81]. The RPTs comprise three C/10 cycles followed by one hybrid pulse power characterization (HPPC) cycle. The HPPC cycle consisted of a series of charge and discharge pulses over a 10% depth-of-discharge interval. The discharge pulse lasts 30 s at 1C and is followed by a rest for 40 s and a 0.75C charge pulse for 10 s [82,83]. In between the RPTs, the cells aged for 30 days at OCV with daily voltage top-up pulses. This testing took place at 45 °C until 80% of the initial capacity was reached. This time ranged from 160–240 days.

2.4. Coin cells for cycle life measurements

Coin cells were also prepared to test the cycle life of cells with low (duplicate cells), moderate (duplicate cells), and high water concentration (triplicate cells). The cells were prepared similarly to the calendar life cells. The anode (d=14 mm) was a polyethylene oxide (PEO) coated Si anode with a copper current collector (t=15 μm). The anode was coated with a wet gap of 100 μm and had a capacity of about 1.5 mAh cm^{-2}. The cathode used in the cycle life cells was a lithium nickel manganese cobalt oxide (NMC 811) (2.59 mAh cm^{-2}) made by the CAMP facility. The N/P ratio was 0.58. The loadings differed in the calendar and cycle life tests in order to match LFP cathodes for the calendar life test and NMC for the cycle life test. LFP was used for the calendar life testing to limit the risk of a high voltage damaging the anode because of transition metal dissolution [84,85] and not provide realistic isolation of Si anode calendar life. The cycle life

tests do not require long periods at a high voltage, so a high-voltage cathode was used. The hardware on the cathode side was Al-clad (MTI). The cells were cycled in a temperature controlled chamber (Maccor) at 30 °C. They were formed with three C/10 cycles and were then cycled for 1000 cycles at C/3 (3–4.1 V). For coin cells used in both calendar and cycle life testing, heterogeneity of hand-coated electrode mass loadings resulted in substantial punch-to-punch variability. This variability is further exacerbated in the Si system because of Si's sloped voltage profile. Slight variations in loading have a larger impact on capacity and performance compared to a graphite system, which has a flat voltage profile, which minimizes the effects on performance of loading variations. The trends discussed in this research are expected to hold when using a more consistent roll-to-roll coated electrode, and better uniformity would reduce cell-to-cell variability.

2.5. Cyclic voltammetry

Cyclic voltammetry (CV) tests were conducted to evaluate oxidative stability of each electrolyte with moderate and high water concentrations. Coin cells were assembled in duplicate and tested using a CV method. The cells were assembled with identical hardware to the coin cells used for cycle life measurements (UMC Corp. and MTI). The negative electrode was a Li disc (Sigma Aldrich, d = 15 mm, t = 0.5 mm), and the positive electrode was a Al spacer (MTI, d = 15.5 mm, t = 0.5 mm). A Celgard 2325 separator was used in the cell (d = 19 mm). The cells were filled with 40 μL of electrolyte.

The CV tests were conducted with a Gamry 1010 potentiostat. The cells were tested at three different potential ranges, 3–4.2 V, 3–4.5 V, and 3-5 V. They completed three scans for each potential range with a scan rate of 100 mV/s.

2.6. Synchrotron infrared nanospectroscopy

Synchrotron Infrared Nanospectroscopy (SINS) was used to evaluate SEI formation in situ.

2.6.1. Electrochemical testing

Si thin film electrodes were evaluated electrochemically in two-electrode pouch cells, using Li metal foil (13-mm diameter, 1.0-mm thickness, MTI Corporation) as the counter and reference electrode with a Celgard 2635 separator (20-mm diameter). The pouch cells were assembled in poly foil bags (Sigma Aldrich, Z183385) cut into 5.5 cm × 6 cm sections. Nickel tabs were used to provide electronic wiring to the electrodes and each cell was heat sealed with adhesive polymer tape (MTI Corporation, EQ-PLiB-NTA4). The cells were filled with 10 μL of the electrolyte. All cell assembly was performed in an Ar-filled glove box with O_2 and H_2O below 0.1 ppm. After cell assembly, light mechanical pressure was applied to the cell with a clamp. Electrochemical cycling with CV or galvanostatic methods were performed with a Biologic VMP3 potentiostat. For characterization, the cells were disassembled in the glovebox and the electrodes were characterized without washing.

2.6.2. Synchrotron IR characterization methods

SINS and atomic force microscopy (AFM) measurements were conducted with a Neaspec neaSCOPE microscope housed at the Advanced Light Source (ALS) at beamline 2.4 using PtIr-coated AFM probes from Neaspec. The microscope is housed in an environmental chamber continuously purged with N_2 and measurements were performed at O_2 < 20 ppm (PureAire, Trace Oxygen Analyzer 0-1000 ppm). AFM topography images were recorded in tapping mode using a tapping amplitude of 5 −60 nm. Images were processed using Gwyddion [86].

SINS spectra were taken with a tapping amplitude of 50–60 nm with a spectral resolution of 16 cm^{-1}. Near-field IR nanoimages, "IR white-light images," were collected simultaneously with the AFM topography measurements by fixing the interferometer mirror position to the most intense feature of the interferogram and recording the resulting second harmonic of the optical amplitude value at each spatial pixel. Reference spectra were taken on a polished Si wafer. Spectra were processed using neaPLOT (neaspec). All spectra were demodulated at the n = 2 harmonic. It is common in the literature to find either the phase, or imaginary part, of the complex nano-FTIR spectrum reported as absorption. This is because in the small angle/phase approximation, the two are mathematically proportional to one another. In this work, strong resonances marked by significant phase responses are frequently measured. The present research reports the second harmonic of the imaginary component of the complex valued nano-FTIR spectra normalized to Si as nano-FTIR absorption. This, because in these strong resonant cases, the imaginary part most closely matches FTIR absorption data bases [87].

2.7. FTIR

FTIR measurements of electrolytes with low, moderate, and high water concentrations were compared to determine whether the presence of water resulted in differences in solvation behavior. The measurements were conducted using a Thermo Fischer iS50 FTIR and Pike GladiATR with a flow-through attachment to limit air contact with the electrolyte samples. Approximately 0.5 mL of electrolyte was injected into the flow-through attachment, and the attachment was capped before data collection started. Each measurement took approximately one minute. The detector was deuterated triglycine sulfate (DTGS) with a resolution of 4 cm^{-1} and a 32-scan average.

2.8. Advanced Electrolyte Model (AEM)

An advanced electrolyte model (AEM) was used to compare electrolyte properties with moderate (300 ppm in this case) and high (1000 ppm) water. The AEM utilizes molecular-scale chemical physics and is based on the mean spherical approximation. This allows for a range of population densities, species-level associations, and analysis of solvent and solution permittivity. The AEM can account for wide ranges of salt concentration and temperature, as well as mixtures of up to ten solvents and two salts. The model yields 20 output reports that cover thermodynamic and transport properties, as well as solvation behavior, microstructure, rheology, and thermo-physical properties [73,88].

2.9. Molecular dynamics

Classical molecular dynamics (MD) simulations were conducted to evaluate the effects of water on electrolyte solvation behavior. MD simulations were carried out using optimized geometries and partial charges derived from density functional theory (DFT) calculations. MD simulations . The geometries of the TMS, DME, and TTE solvents, as well as the FSI^- anion, were optimized using Q-Chem version 6 [89] at ωB97X-V/ cc-pVTZ level of theory. Partial atomic charges obtained from the geometry-optimized molecules using RESP method and subsequently assigned to each molecule for use in the MD simulations. All MD simulations were performed through OpenMM [90] using the atomate2 [91] workflow. Initial simulation boxes were generated with Packmol [92] to pack solvent molecules and ions according to the desired stoichiometry. Each dry electrolyte system contained a total of 3000 molecules. For the wet electrolyte systems, 1000 ppm water was added to the corresponding dry composition. The non-polarizable Sage force field [93] was employed for all simulations. To account for the lack of explicit electronic polarization in such force fields, the partial charges of Li^+ and FSI^- were uniformly scaled by a factor of 0.8, a common correction used to mitigate the overestimation of electrostatic interactions [94,95]. Energy minimization was first performed with a force cutoff of 10 kJ mol^{-1} nml^{-1}. This was followed by equilibration in the isothermal–isobaric (NPT) ensemble for 10 ns at 298 K and 1 atm using a Monte Carlo barostat. Subsequently, the systems were subjected

to a 45 ns annealing protocol, starting with a 15 ns ramp up from 298 K to 400 K, followed by 15 ns hold at 400 K, and 15 ns ramp down to 298 K. Production trajectories were then generated under the canonical (NVT) ensemble for 80 ns at 298 K, employing a Langevin Integrator thermostat. Periodic boundary conditions were applied in all directions. Solvation structure analyses were carried out on the equilibrated NVT production trajectories. This was done using the SolvationAnalysis [96] package, which is built on the MDAnalysis Python library [97]. A simulation timestep of 1 fs was used.

2.10. NMR

NMR data were collected to measure solvation and degradation products of electrolytes with moderate and high water concentrations. The electrolyte with high water concentration was aged for six months. Samples were prepared by adding 800 μL of the each prepared electrolyte (LiFSI 3TMS/3TTE and LiFSI 1.2DME/3 TTE) to an NMR tube with an insert containing 100 μL of DMSO-d_6 and para-fluorotolulene. The aged electrolyte measurement was made by taking an aliquot from the aging electrolyte container. All samples were measured by a Avance Bruker 300 MHz NMR with 8 scans.

3. Results

3.1. Calendar life

Calendar life tests revealed that cells containing LHCEs with moderate water concentration exhibited about 8% higher capacity retention (1200–1300 mAh/g Si) than cells containing LHCEs with water removed (Fig. 2, S1, S2). While cells with both high and low water concentration had similar trajectories after two to four RPTs, the cells with high water content diverged between 50–100 days of calendar life testing. The cells with low water content began a downward sloping path and exhibited a reduction in capacity retention below 80% between 160 and 200 days. The cells with moderate water content retained greater than 80% beyond 200 days of calendar life testing, though they did begin a sharper downward capacity curve around 150–160 days. The moderate concentrations of water in the electrolyte did not result in catastrophic degradation, instead improving capacity retention or at least delaying capacity fade. To understand the role of water in this system of Si anodes paired with LHCEs, this research considers how the presence of water may exacerbate electrolyte oxidation, modify the SEI composition, or change the electrolyte's solvation structure or composition.

Water could exacerbate electrolyte oxidation by behaving as a sacrificial oxidant, where it could bolster the Li inventory of a cell by converting Li-ions in the electrolyte into Li-ions in the cyclable lithium inventory. While masquerading as shorter term capacity retention, electrolyte oxidation results in long-term cell degradation due to electrolyte degradation and loss [98,99]. Endpoint slippage analysis and CV testing were used to assess water's role in electrolyte oxidation.

Water or a product formed from a reaction with water could behave similarly to other electrolyte additives and alter the chemical or mechanical stability of the SEI to affect performance. Many electrolyte additives alter the SEI through a variety of mechanisms, including increasing the proportion of inorganic species, promoting polymeric cross-linking, and improving mechanical flexibility among other pathways [100–104]. Synchrotron Infrared Nanospectroscopy (SINS) was used to understand the effects of water on the SEI.

Finally, because of its highly polar nature, water could also favorably change the solvation structure of the electrolyte. Water's role in lithium ion solvation and resulting effects on cell performance have been studied particularly for electrolytes in which water is native to their design, such as water-in-salt and hybrid aqueous/non-aqueous electrolytes [105–108]. FTIR spectroscopy, an Advanced Electrolyte Model (AEM), molecular dynamics simulations, and NMR spectroscopy were utilized to evaluate water's influence on solvation structure in the electrolyte

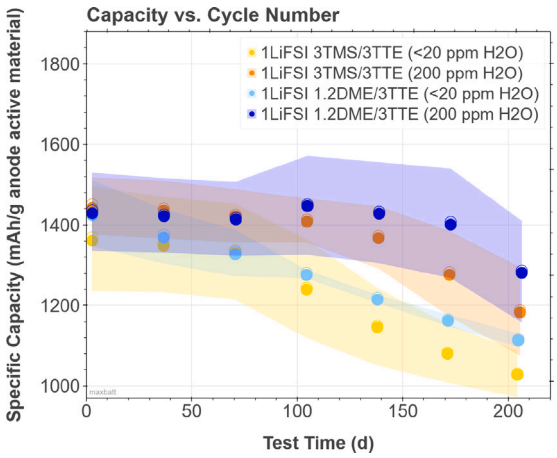

Fig. 2. Calendar life tests were conducted with 2032 coin cells containing a Si-based anode (1 mAh cm^{-2}) and an LFP cathode (1.88 mAh cm^{-2}). The shaded regions represent the standard deviation of specific capacity for each cell group. Cells underwent a calendar aging cycling protocol at 45 °C. LHCEs with water concentrations around 200-300 ppm demonstrated improved specific capacity, areal capacity, and capacity retention over LHCEs with dried electrolytes.

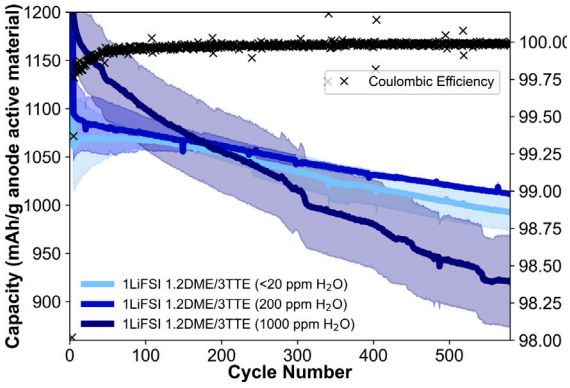

Fig. 3. Cycle life tests were conducted with 2032 coin cells containing a Si-based anode (1.5 mAh cm^{-2}) and a NMC cathode (2.59 mAh cm^{-2}). Cells underwent a cycle life testing protocol (C/3 charge and discharge) at 30 °C. The shaded regions represent the standard deviation of specific capacity for each cell group. The DME-based LHCE with water concentrations around 200-300 ppm demonstrated improved specific capacity, areal capacity, and capacity retention over the LHCE containing dried solvents.

3.2. Cycle life

Cycle life tests indicated general water tolerance up to 1000 ppm for both DME and TMS based LHCEs with subtle difference depending on the system. Figs. 3, S3 and S4 show the impact of water on the cycle life performance of the DME-based electrolyte. Moderate water concentration does not appear to have major negative impacts on cycle life performance in metrics of specific, relative, and areal capacities, as well as Coulombic efficiency. Cells with low water and moderate water concentration maintained a linear downward trajectory in capacity after the first 50 cycles and maintained > 80% of initial capacity over 600 cycles. Cells with high water concentration lost greater capacity compared to cells with low and moderate and maintained a steady capacity decline during the test. These cells reached 80% capacity within only 400 cycles.

This result may indicate a moderate "water tolerance" of the DME-based LHCE. While cells containing dilute carbonate-based electrolytes may exhibit rapid capacity fade due to a small amount of water [12,15],

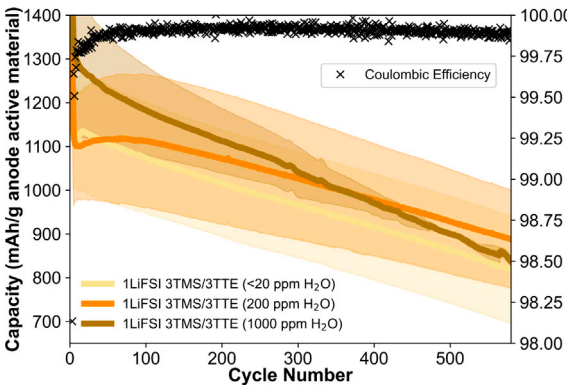

Fig. 4. Cycle life tests were conducted with 2032 coin cells containing a Si-based anode (1.5 mAh cm^{-2}) and a NMC cathode (2.59 mAh cm^{-2}). Cells underwent a cycle life testing protocol (C/3 charge and discharge) at 30 °C. The shaded regions represent the standard deviation of specific capacity for each cell group. The TMS-based LHCE with water concentrations around 200-300 ppm demonstrated improved specific capacity, areal capacity, and capacity retention over LHCEs with dried electrolytes during 600 cycles at C/3. The cells in these tests were graphite versus NMC and cycled at 30 °C.

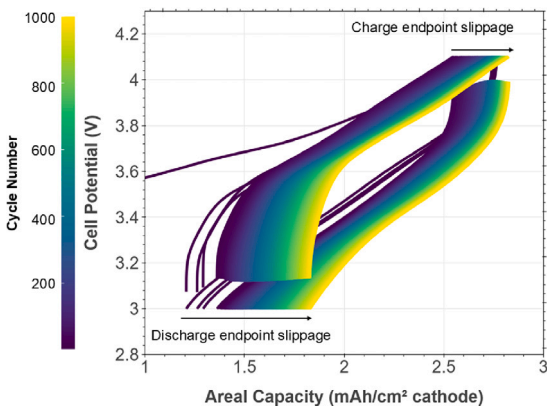

Fig. 5. Cycle life testing from one cell containing a TMS-based electrolyte with moderate water concentration is shown in this plot. Identical testing protocols are shown in Fig. 3 and 4. Endpoint slippage is visible at the top (4.1 V) and bottom (3 V) of charge as cycles proceed.

the DME-based LHCE can perform well even with moderate amounts of water. The LHCE may be tolerant not only of water itself but also of reaction byproducts from water reacting with the Li salt, electrolyte solvent, or SEI components. In the cycle life testing compared to the calendar life testing, the cell experienced far more movement of Li-ions and solvation structure changes, as well as their interaction with the Helmholtz layer that could result in more continual byproduct speciation.

Cycle life tests of the TMS-based electrolyte showed a different result. Figs. 4, S5 and S6 indicate that water up to 200–300 ppm has relatively little effect on cycle life performance. While the capacity trajectory of the DME-based electrolyte with high water concentration sharply declined, the capacity fade of the TMS-based electrolyte with high water concentration was only somewhat steeper than the TMS-based electrolytes with low and moderate water up to 600 cycles. Generally, the DME-based electrolyte performed better overall, however, than the TMS-based electrolyte in cycle life tests. The TMS-based electrolyte with low water concentration reached 80% of initial capacity around 500 cycles, while the TMS-based electrolyte with moderate water concentration reached 80% of initial capacity around 600 cycles. The TMS-based electrolyte with high water concentration reached 80% of initial capacity within about 200 cycles. Examining the oxidative stability, SEI composition, and solvation structures of each LHCE system helps to reveal why there are subtle differences in water tolerance between the DME-based and TMS-based LHCEs.

3.3. Electrolyte oxidation

Electrolyte oxidation could temporarily hide long-term cell degradation. For example, oxidation of water in the electrolyte on the cathode surface leads to the conversion of dissolved Li^+ in the electrolyte to Li^+ in the cell's cyclable inventory (Eq. (2), (3)):

$$2H_2O \longrightarrow 4H^+ + O_2 + 4e^- \quad (2)$$

$$2e^- + 2Li^+ + Si \longrightarrow Li_2Si \quad (3)$$

In the short-term, cell capacity would appear unchanged or even increasing, but over time, electrolyte species will decompose, which will result ultimately in worsening cell health [109,110]. For example, Rinkel et al. [110] propose a hydrolysis reaction of DMC to form lithium methyl carbonate and methanol. The effect of water on electrolyte oxidation was investigated with two approaches: endpoint slippage and CV measurements.

3.3.1. Endpoint slippage

Endpoint slippage refers to an approach developed by Jeff Dahn's group to measure the contribution of parasitic side reactions to cell capacity fade [80,109,111–113]. Fig. 5 shows a voltage versus capacity plot to illustrate endpoint slippage analysis. During cycling, parasitic reactions will occur at both the anode and cathode sides in the form of SEI growth and oxidation reactions, respectively. To visualize the contribution of these parasitic reactions to the cell capacity, the cumulative capacity can be plotted on the X-axis and the cell potential on the Y-axis. Parasitic reactions at the anode are denoted as discharge endpoint slippage and can be visualized as rightward shift in the capacity at low potentials. These reactions remove electrons and their corresponding Li-ions from the cyclable lithium inventory by forming SEI species, which will then result in a smaller reversible capacity between the cutoff potentials. Parasitic reactions at the cathode are denoted as charge endpoint slippage and are associated with a rightward shift in capacity at high potentials. On the cathode side, water or products formed from reactions with water could oxidize at high potentials. Water oxidation, as shown in Eq. (2) results in extraction of electrons from water and the subsequent conversion of Li-ions in the electrolyte to Li in the cell's cyclable inventory (Eq. (3)). This shifts the upper cutoff potential rightward, resulting in a larger reversible capacity between the cutoff potentials. Thus, endpoint slippage analysis should reveal whether water oxidation is masquerading as cell capacity. Endpoint slippage analysis does have limitations, particularly related to cells with Si-based anodes [80] due to their highly sloped voltage profile.

For the present study, endpoint slippage was determined by subtracting the charge or discharge endpoint at cycle four (first cycle after the 3x C/10 formation cycles) from the charge or discharge endpoint at cycle 580. These values were divided over the cathode loading. Figs. 6 and 7 show the charge and discharge endpoint slippage for each cell replicate. Charge endpoint slippage does not appear to be significantly greater in the DME-based electrolyte with high water concentration. An increase in charge endpoint slippage is correlated with increased water concentration in the TMS-based electrolyte, though the cells with low water concentration did have significant variability in charge endpoint slippage. This may explain the better cycle life performance of the TMS-based electrolyte with high water concentration compared to the DME-based electrolyte with high water concentration. Because both charge and discharge endpoint slippage were observed, another explanation could be a reversible redox shuttle. However, greater endpoint slippage occurred at high potential, so there are likely other factors affecting capacity changes.

Discharge endpoint slippage does show a trend related to water concentration. Although the discharge endpoint slippage is similar

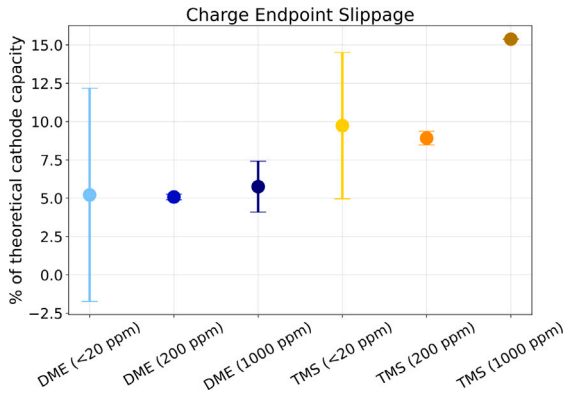

Fig. 6. Endpoint slippage analysis was conducted on cycle life testing data shown in Figs. 3 and 4. Error bars represent the standard error of the mean. Charge endpoint slippage appears to increase when the water concentration of the TMS-based electrolyte is increased from 200-300 ppm to 1000 ppm.

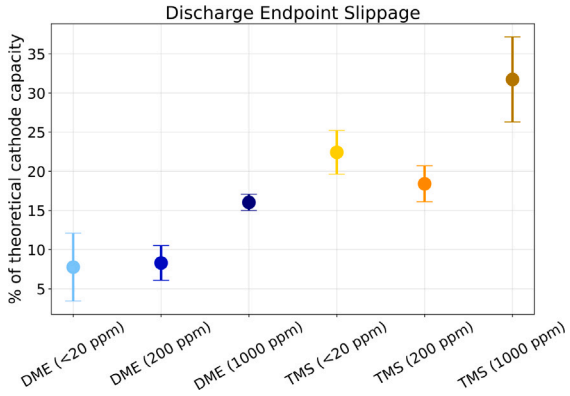

Fig. 7. Endpoint slippage analysis was conducted on cycle life testing data shown in Figs. 3 and 4. Error bars represent the standard error of the mean. Discharge endpoint slippage does appear to correlate with water concentration for both electrolytes.

between low and moderate concentrations for both LHCE systems, electrolytes with high water concentration have slightly higher discharge endpoint slippage. This indicates that greater SEI growth may be occurring in cells with high water concentration. Greater SEI growth may result from continual damage to the SEI and subsequent regrowth that ultimately results in capacity fade. While continual SEI growth is a concern more broadly, SEI growth would not temporarily bolster Li inventory, so it is not a possible mechanism to explain the better calendar life performance of cells with moderate water concentration. The trend of discharge endpoint slippage does matter for cell performance but not in the present comparison of electrolytes with varying water concentrations.

3.3.2. Cyclic voltammetry

CV tests were conducted to compare oxidative stability of electrolytes with different water concentrations. Water in the electrolyte had mixed effects on the oxidative stability. Cycling and calendar life tests were conducted with an upper voltage cutoff of 4.1 V, but oxidative stability was measured up to 5 V to find a realistic upper limit. Fig. 8 shows the average maximum current measured during the three scans conducted at each voltage limit.

At all three potentials, the cell containing TMS-based electrolyte with high water concentration had a greater current at high potentials, indicating more oxidation reactions, compared to the TMS-based electrolyte with moderate water. Conversely, the DME-based electrolyte

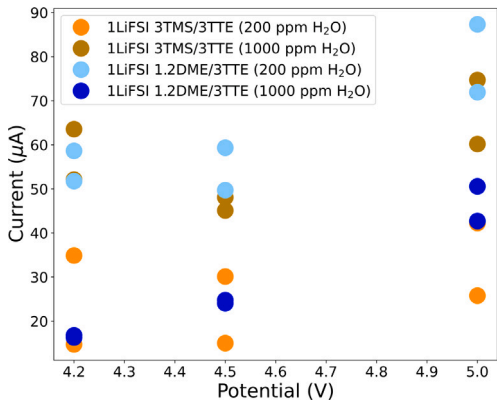

Fig. 8. Cyclic voltammetry (CV) tests were conducted in 2032 coin cells with an Al working electrode and Li counter electrode. Duplicate CV tests were conducted for each sample, and both results are shown. The cells underwent voltage sweeps from a minimum potential of 3 V and maximum potentials of 4.2, 4.5, and 5 V. Sweeps were conducted at 100 mV/s. CV tests revealed that water in the electrolyte has varying effects on oxidative stability. A high water concentration (1000 ppm) in the DME-based electrolyte improved oxidative stability over a moderate water concentration (200-300 ppm), while a high water concentration in the TMS-based electrolyte worsened oxidative stability.

with a high water concentration showed improved oxidative stability, compared to the DME-based electrolyte with moderate water. The higher oxidation currents indicate that water oxidation may be masking capacity fade more than in a cell with lower oxidation current. This result is congruent with the better cycle life performance and greater charge endpoint slippage of the TMS-based electrolyte with high water concentration relative to the performance disparity between the DME-based electrolytes with low, moderate, and high water concentrations. A caveat exists in that a Li metal counter electrode was used in the CV experiments. The interaction of the Li metal electrode with water could result in new products or products at higher concentrations than found in the cells with no Li metal electrode. However, because the results of the CV tests agree with the results of the cycle life tests, the Li metal electrode likely does not confound this comparative test between the two electrolytes. Agreement between the results of the endpoint slippage analysis, which used realistic electrodes, and the CV tests, which used Li metal electrodes, support the validity of the CV tests for comparing oxidative stability of the electrolytes. Additionally, in commercial cells where electrolyte lean conditions are used and other harmful effects of oxidation such as gassing must be considered, the DME-based electrolyte could have fewer side reactions and would likely exhibit better long term performance when high water concentrations are present.

3.4. SEI characterization

The presence of water could affect the calendar aging performance by altering the chemical or mechanical properties of the SEI. To assess the effect of water in the TMS-based electrolyte on the SEI, SINS was performed to characterize the nanoscale topography and chemistry of the SEI layer on model Si thin films. By implementing a synchrotron source coupled with a He-cooled detector, low frequency vibrational modes (600–300 cm^{-1}) originating from Li inorganic phases (such as Li_2O and LiF) can be observed allowing for both organic/molecular vibrations and inorganic modes to be detected in the SEI layer with 20-nm scale spatial resolution [114].

IR nanospectroscopy revealed chemical and structural differences in SEI. The 50-nm thick a-Si thin film electrodes were first cycled five times between 0.05 V and 1.50 V at 0.1 mV/s and then held at 0.05 V for 45 h to assess their parasitic currents (Fig. S7) [115].

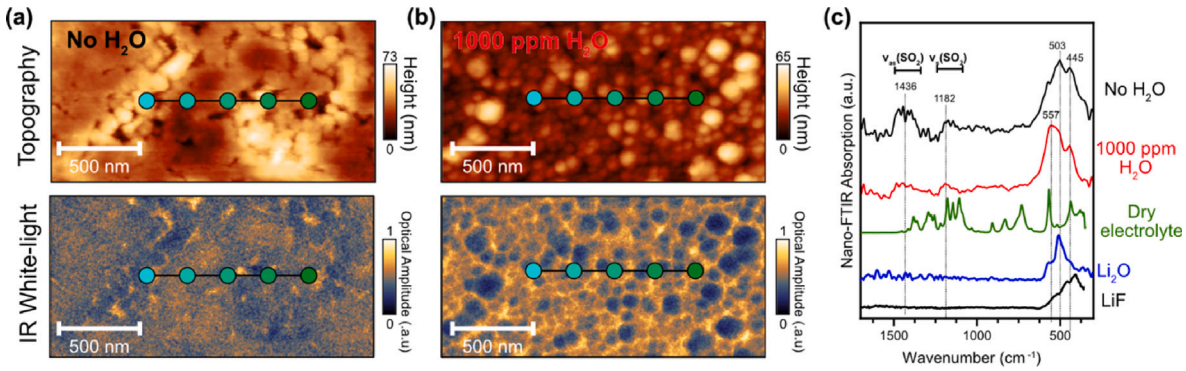

Fig. 9. AFM topography and IR white-light image of the a-Si thin film electrode after 5 CV cycles at 0.1 mV/s from 0.05–1.50 V followed by a 45-hour voltage hold at 0.05 V in the (a) low water electrolyte and (b) the same electrolyte spiked with 1000 pm of H_2O. (c) SINS spectra averages of the linescans shown in (a,b) along with references from the electrolyte with low water concentration and Li_2O and LiF (from Ref. [114]).

Both electrodes showed the typical behavior of a-Si alloying reactions; however, the high-water-concentration electrolyte exhibited a higher cell resistance possibly related to modified SEI formation on the Si or Li metal electrodes. After the 45-hour hold, the electrolyte with high water concentration resulted in a lower parasitic current of 0.064 μA/cm^2 compared to 0.106 μA/cm^2 suggesting that the additional water improved the passivation.

After the voltage hold, the thin film electrodes were characterized with AFM topography, IR white-light imaging and IR nanospectroscopy to determine any differences in the nanoscale topography and chemistry of the two SEI layers. The topography (Fig. 9a, top) of the electrolyte with low water concentration appears relatively smooth with small cracks. The corresponding IR white-light image (Fig. 9a, bottom), which is sensitive to the nanoscale reflectivity of the near-field IR light, is homogenous across the surface which is an indication of chemical uniformity on the nanoscale. In contrast, the SEI formed with the high-water-concentration electrolyte, exhibited an SEI topography consisting of nanoparticles approximately 50–100 nm in size across the surface indicating the water seemed to modify the resulting topology of the SEI layer.

Fig. 9c shows the nano-FTIR spectra averages from the linescan in Fig. 9a,b along with the ATR-FTIR spectrum of the dry electrolyte along with reference spectrum of Li_2O and LiF. Both linescans across the surface (Fig. S8) showed similar spectra, suggesting that both SEI layers are chemically homogenous on the nanoscale (consistent with the IR white-light images). Both nano-FTIR spectra from the surface exhibit broad peaks around 1436, 1182 and 500 cm^{-1} but with different ratios. The absorption at 1436 and 1182 cm^{-1} can be attributed to asymmetric and symmetric stretching modes related to SO_2 groups, respectively [116,117] . These groups are present in the original electrolyte (from the FSI and TMS) but the other vibrational modes such as S-N-S (567 cm^{-1}) appear to be absent or attenuated in the SEI layer. The broad feature around 500 cm^{-1} dominate the spectrum with a higher ratio in the 1000-ppm-water electrolyte. This peak is typical of Li-ion inorganic phases as observed in previous work [114]. Based on comparing the peak position with the Li_2O and LiF references, the SEI layer appears to be composed of primarily Li_2O along with some S–O groups as evidenced by the peaks at 1435 and 1182 cm^{-1}. The effect of high water in the electrolyte appears to alter the topography of the SEI layer along with increasing the relative ratio of Li_2O to S–O related groups. Although determining the contribution of any one SEI component to cell performance is challenging and beyond the scope of this work, water in the electrolyte did affect SEI chemistry and structure. Water did increase the relative amount of Li_2O in the SEI, and Li_2O has been associated with interface stability in high-energy electrodes [118–121]. Two caveats exist for this experiment: (1) a Li metal counter electrode was used instead of NMC or LFP and (2) a Si thin-film anode was used instead of a composite Si electrode. The Li metal electrode may have influenced the type or concentration of SEI components measured on the Si anode. The thin-film Si anode excludes electrolyte interactions with the higher surface area carbon and binder. This measurement, however, is not intended to provide a perfectly representative profile of the SEI in the SI composite anode. Rather, this measurement is intended to determine whether substantial water concentration in the electrolyte generally affects SEI products that form. The calendar life results support a high water tolerance of these electrolytes, which could be caused by advantageous SEI products, such as Li_2O, which is present in greater quantities in the SINS experiment with high water concentration.

3.5. Electrolyte solvation and composition

Long-term differences in electrolyte solvation and composition could account for variability in calendar life performance. Electrolyte solvation structure is critical for cell cycling and long-term stability [122]. FTIR, electrolyte modeling, and molecular dynamics were used to evaluate solvation structure. NMR was utilized to evaluate both solvation structure and electrolyte composition.

3.5.1. FTIR

FTIR spectra were measured from electrolytes with low, moderate, and high water concentrations. TMS-based electrolytes and the DME-based electrolytes showed almost no differences between different water concentrations (Fig. S9, S10, and S11). The vibrational modes studied were chosen based on previous literature studies of electrolytes with TMS (SO_2 bending and CH_2 bending) [123] and DME (C-O-C bending) [62]. This result is consistent with computational models and NMR.

3.5.2. Advanced electrolyte model

The AEM architecture determines preferential solvation for free (non-associated) cations and anions. That is, it calculates the probability of finding a given solvent in the primary solvation shell of a chosen ion, given the bulk electrolyte formulation, salt concentration, and temperature. The probability functions are tied to the relative molar proportions of solvent, the ion populations, the solvent residence times for all solvents in relation to the ions, and other thermodynamic terms. Preferential ion solvation is not a static quantity, as it can vary over salt concentration due to the solvent availability in bulk versus the competition for solvent as occupants of solvation shells. The LHCE system LiFSI 3TMS/3TTE was modeled with 300 versus 1000 ppm water at 25 °C. Fig. 10b shows the preferential cation solvation by the three solvents over salt concentration, as expressed as solvent mole fractions within the lithium solvation shells. First, TMS is seen to be the preferred solvator at a 2:1 molar proportion over TTE. This preference increases slowly to 2.8:1 at the higher salt concentrations. The cation

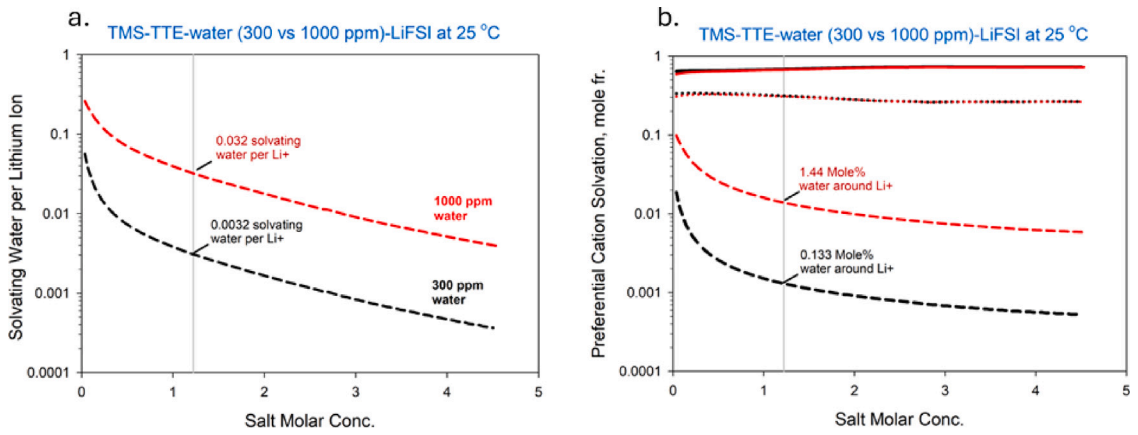

Fig. 10. AEM comparison of metrics for preferential lithium solvation by water, comparing cases of 300 versus 1000 ppm water in the solvent mixture. Panel (a) solvating water molecules per lithium ion and (b) shows the water mole fraction in lithium solvation shells.

solvation number decreases over salt concentration. The behavior for water shows a marked decrease over salt concentration, owing more to the trace amounts of water and the dilution effect caused by the increasing ion population. At 300 ppm water, there is 0.133 mole percent water in cation solvation shells at the design concentration of 1.22M salt, while that amount increases to 1.44 mole percent for the 1000 ppm case.

Additionally, there is an enrichment of water in the lithium solvation shell volumes versus the bulk solvent. At 300 ppm water, the mole fractions for solvent mix of TMS:TTE:water are 0.49723:0.49984:0.00293 at 25 °C, where in Fig. 10(a) the water mole fraction in the cation solvation shells exceeds 0.00293 until 0.44M. In comparison, at 1000 ppm water, the mole fractions for solvent mix of TMS:TTE:water are 0.49386:0.49646:0.00969, where in Fig. 10(a) the water mole fraction in the cation solvation shells exceeds 0.00969 until 2.1M.

Since AEM also provides the solvation number for cations over salt concentration, the result from panel (a) can be multiplied times the solvation number to derive Fig. 10(b), which shows the solvating water molecules per lithium ion. At the design salt concentration of 1.22M, there is 0.0032 water molecules per lithium ion at 300 ppm water, which increases an order of magnitude to 0.032 for the 1000 ppm case. This equates to 1 in 312 lithium ions will contain one water molecule when 300 ppm water is present in the bulk electrolyte, but 1 in 31 lithium ions will carry a water molecule when 1000 ppm is present. While 300 to 1000 ppm water is a relatively low concentration in the electrolyte, the AEM indicates that water disproportionally participates in solvation. This magnifies the electrochemical effects of water in the electrolyte. For example, water may be overrepresented as an SEI reactant because of solvation effects.

3.5.3. Lithium solvation energy comparison

Solvation energies are another metric which can indicate the relative strength of interactions between solvents and ions. Since the electrolytes studied have trace amounts of water (300 vs 1000 ppm), it is anticipated that a single cation is not likely to be fully solvated by water, but instead have a single water molecule in its solvation shell along with TMS and TTE. Thus, AEM was used to study the single-solvent solvation energy between Li^+-water$_1$ and Li^+-TMS$_1$, since TMS has been shown to be a more aggressive solvator than TTE. AEM provides a rigorous chemical physics platform to determine solvent-to-ion binding energies and related solvation numbers, covering the complete thermodynamic cycle necessary for describing the solvation process. At 25 °C and low-to-moderate salt concentrations, the Li^+-water$_1$ binding energy is predicted at 151.0 kJ/mole, while that for Li^+-TMS$_1$ is 227.4 kJ/mole. The latter value agrees well with 227.7 kJ/mole found in the literature [124]. Thus, for a mixed-solvent solvation shell environment, water would undergo desolvation earlier than TMS. This infers that water could well be carried by lithium ions toward an electrode surface, but would become decoupled from the ions prior to the other solvators, and may not actually be transported all the way to the inner SEI or surface due to Faradaic currents. As such, water could accumulate in and near the Helmholtz region where it could play a role in SEI stability or eventually be consumed in passivation processes. This result agrees with the nano-FTIR results showing greater Li_2O, likely a product originating from water consumption, in the SEI for an electrolyte with high water concentration.

3.5.4. Molecular dynamics

MD was used to evaluate the coordination environment for electrolyte with high water concentration. Analysis of the MD trajectories reveals that the addition of 1000 ppm water does not substantially modify the local coordination structure around Li^+ in either the LiFSI 3TMS/3TTE or the LiFSI 1.2DME/3TTE electrolyte. In both systems, TTE acts as a non-coordinating diluent and contributes negligibly to the first solvation shell (<0.01). TMS and DME act as coordinating solvents, with TMS binding much more strongly to Li^+ than DME. This is shown in the average composition of Li^+ first solvation shell, illustrated in Figure S12.

In the LiFSI 3TMS/3TTE system, the coordination environment remains essentially constant: Li^+- FSI^- coordination shifts only from 1.13 to 1.12, and Li^+-TMS coordination, which dominates the solvation shell, remains at ~3.90 at both 0 and 1000 ppm water. Similarly, in the LiFSI 1.2DME/3TTE system, the effect of 1000 ppm water is negligible, with Li^+-FSI^- coordination changing from 3.85 to 3.80, and Li^+-DME coordination increasing slightly from 0.42 to 0.43. In both water-containing electrolytes, minimal Li-H_2O coordination is detected (<0.01), due to the low absolute concentration of water. These minor variations fall within the statistical uncertainty of MD simulations.

To further probe the possibility of micelle-formation in these electrolytes, FSI^- ion-pairing states using were classified using the definitions from Efaw et al. [76] where the coordination environment is defined by the number of Li^+ ions coordinated to FSI^- anions. SSIPs denotes 0 Li^+ coordination, CIPs denotes 1 Li^+ coordination, AGG denotes 2 or 3 Li^+ coordination, and AGG+ denotes 4 or more Li^+ coordination. As shown in Figure S13, the ion-pairing distributions remain essentially unchanged upon the addition of 1000 ppm water in both electrolytes.

In the LiFSI 3TMS/3TTE system, the strong coordination affinity of TMS for Li^+ likely stabilizes compact clusters and suppresses the formation of large micelles, as indicated by the minor AGG+ fraction of ~ 2% in both dry and wet electrolytes. This is illustrated in the MD snapshot in Fig. 11a, which shows small LiFSI clusters dispersed throughout the simulation box.

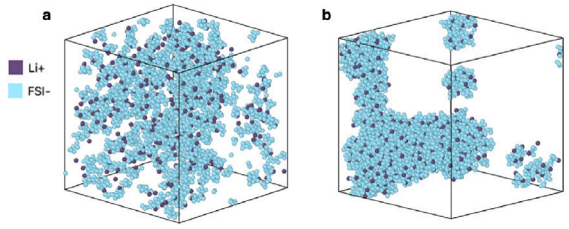

Fig. 11. Representative MD simulation snapshots of Li^+-FSI^- ion clustering behavior in (a) 1:3:3 LiFSI:TMS:TTE, where small clusters remain dispersed throughout the simulation box, and (b) 1:1.2:3 LiFSI:DME:TTE, where large LiFSI clusters percolate across the simulation cell.

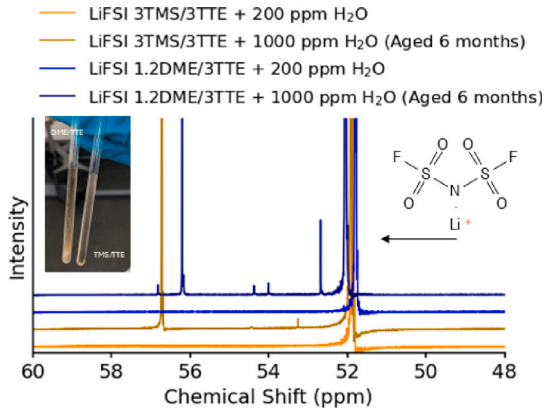

Fig. 12. ^{19}F NMR spectra indicate some LiFSI degradation. Integration of the primary LiFSI peaks and surrounding peaks indicated differential amounts of LiFSI degradation between the DME/TTE and TMS/TTE electrolytes, 15% and 6%, respectively.

In contrast, in the LiFSI 1.2DME/3TTE system, AGG+ dominate, making up to 79% of the solvation environment. The weak coordination of the ether oxygen in DME encourages preferential interaction of Li^+ and FSI^-, forming large LiFSI cluster that spans the simulation box. This is shown in Fig. 11b. Overall, MD simulations show no meaningful changes in either the lithium solvation environment or the ion-pairing distributions upon the addition of 1000 ppm water to both electrolyte systems. The discrepancy with the experimental observations are likely due to the formation of new species through chemical reactions occurring within the electrolyte, which are not captured by classical MD simulations. The limited time-scale and system size of MD may be insufficient to capture larger length-scale effects that are observed experimentally. Surface effects were also not considered in these simulations and this could play a significant role in SEI and cathode/electrolyte interface dynamics.

Both the AEM and MD simulations indicate negligible effects on the coordination environment by water at up to 1000 ppm, which is consistent with the low absolute concentration of water in the electrolytes.

3.5.5. NMR

NMR was utilized to measure solvation and composition of electrolytes with moderate and high water concentrations. The electrolyte with high water concentration aged for six months at ambient temperature.^1H NMR spectra were collected both samples, and no peak shifts were observed (Fig. S14). This indicates that no large-scale differences in the coordination environment exist between cases.^{19}F NMR spectra do show some degradation of LiFSI (Fig. 12).

The LiFSI peak ($\delta_F \approx 52$ ppm) is associated with the $F-SO_2^-$ group of FSI^- [74] and is strongly visible in both the low water electrolyte and the high water/aged electrolyte. For both the TMS/TTE and DME/TTE electrolytes, other peaks around 52-57 ppm appeared after eight weeks of aging at room temperature. Some discoloration and crash out was visible. The FSI^- peaks and surrounding peaks were integrated with the MestReNova software. The integrated area of peaks between 50-58 ppm was given an arbitrary value of 1. The FSI^- peak at 52 ppm was then integrated by itself, and then the remaining peaks in the 50-58 ppm region were integrated. The area of the FSI^- peak divided by the total area of all the peaks in the 50–58 region is presumed to represent non-degraded FSI^-. Those values differed between the TMS/TTE and DME/TTE of electrolytes. The TMS/TTE electrolyte retained about 94% of non-degraded FSI^-, while the DME/TTE electrolyte retained about 85% of non-degraded FSI^-. These data show that some degradation can occur because of chemical reactions between water and the electrolyte salt and solvents. Electrochemical effects may cause further degradation.

In a separate set of NMR measurements, a singlet was observed in the ^1H spectrum starting near 3.4 ppm [125] for both the TMS-based and DME-based electrolytes (Fig. S15–S18). The singlet did shift downfield in both cases after one week of aging likely due to the usage of DMSO d-6 directly in the electrolyte, which caused some solvation change over time, instead of in an insert, which was used for the previously discussed NMR experiments. The singlet did, however, have the same integrated intensity for the electrolyte samples with 1000 ppm of water added. This result indicates that water did not completely react into different products while in the electrolyte itself, but possible degradation and solvation change due to the presence of DMSO-d_6 did cause downfield shifting. Although water may exist in the electrolyte itself for extended periods, the water will likely react rapidly in a cell setting because of its limited electrochemical stability window [126].

The AEM, MD, and NMR results suggest no effect of water on the coordination environments of either the TMS/TTE or the DME/TTE electrolytes. The AEM results indicate, however, that water may have an outsized effect on electrochemical processes such as SEI formation. This is because it may be overrepresented in solvation spheres, compared to its bulk concentration. NMR results show that some anion degradation is possible after several weeks of aging, though the degradation is < 15% of the initial salt concentration for both electrolyte systems.

3.5.6. Comparison with a dilute electrolyte system

Experimental and modeling efforts suggest that both the TMS-based and DME-based are highly water tolerant even up to 1000 ppm water in some cases. The electrolytes studied have two qualities that encourage stability: (1) they both contain LiFSI salt, which is not known to hydrolyze under standard battery operating conditions [30] and (2) they utilize a LHCE design, which is stable versus highly reactive electrodes, such as Li metal [65–67]. To differentiate between the contributions of the LiFSI salt and the LHCE design, additional cycle life tests were conducted using 1M LiFSI in 3/7 EC/EMC (wt./wt.) and 1.2M $LiPF_6$ in 3/7 EC/EMC (wt./wt.) + 3 wt% fluoroethylene carbonate (FEC) electrolytes. Half of the cells tested had 1000 ppm water added to the electrolyte. Figures S19 and S20 show that the capacity of the cells containing 1M LiFSI in 3/7 EC/EMC (wt./wt.) and 1.2M $LiPF_6$ in 3/7 EC/EMC (wt./wt.) + 3 wt% FEC declined rapidly. These results suggest several important conclusions: (1) LiFSI is highly water tolerant because adding water does not affect cell performance in either the LHCE or dilute cases; (2) the LHCE design is critical for stabilizing the Si-based cell system because both dilute electrolyte systems tested failed rapidly.

4. Conclusion and discussion

The present study reveals that LHCEs promote capacity retention in cycle and calendar life testing of Si-based cells, despite the presence of a known impurity. Although previous research on Si anodes indicated

water in the electrolyte may be the root cause of cell failure [6,7], water had unexpected positive effects on calendar life for two different LHCEs. Also, water at a 200-ppm concentration had little effect on cycle life performance, and even 1000 ppm of water did not result in rapid capacity fade. In a long-term cell cycling test, however, water should be limited to 200 ppm or less to minimize degradation. These results suggest that the relationship between electrolyte chemistry, impurities, and cell performance is more complex than previously understood.

In this research, three causal mechanisms were investigated: (1) electrolyte oxidation temporarily bolstering cell capacity, (2) water acting as a beneficial reactant for SEI chemical stability, (3) water playing a role in a more favorable coordination environment. This study revealed water impacted both the structure and chemistry of the SEI. The presence of 1000 ppm water in the electrolyte increased the proportion of Li_2O in the SEI. Although determining the exact effects of any one SEI component is beyond the scope of this study, previous research has shown beneficial effects of Li_2O on cell performance [41–43]. Electrolyte modeling results supported the SINS measurement of SEI: despite the low overall water concentration, water could disproportionally affect SEI reactions because of its overrepresentation in the solvation structure. Electrolyte models did not support a large-scale change in the electrolyte coordination environment. CV tests and endpoint slippage analysis ruled out electrolyte oxidation masquerading as cell capacity. This implies that the LHCEs in this study have a legitimate, lasting impurity tolerance in both continuous cycling and high voltage hold conditions.

One caveat to these results is that these systems did have excess electrolyte. Excess electrolyte could have impacted cell performance and longevity in a few different ways. Excess electrolyte could prolong cell life- time by minimizing impedance rise due to electrolyte dry-out [127]. Excess electrolyte could also dissolve the SEI and reduce cell life more rapidly compared to an electrolyte lean system. Although the present study should be extended to a lean electrolyte system for more commercial relevance, water in the electrolyte resulted in surprising cell performance when compared across electrolyte-rich systems.

These results are impactful not only for this specific system but also for electrolyte development broadly. The present study reveals that a common impurity at a relatively low concentration potentially affects SEI structure and chemistry while retaining cycle and calendar life. Even small changes to the LHCE solvent and impurity concentrations could have important mechanistic effects. Finally, the present study undergirds the promise of LHCEs in highly reactive battery systems. Battery systems beyond graphite/NMC offer greatly increased capacity, though at the cost of reactivity. Even with water present, these LHCEs did not react and degrade as expected. Overall, LHCEs represent a path forward to broadening battery chemistries to increase energy density and cell lifetimes.

CRediT authorship contribution statement

Lydia Meyer: Writing – review & editing, Writing – original draft, Visualization, Methodology, Investigation, Formal analysis, Data curation, Conceptualization. **Marco-T.F. Rodrigues:** Methodology. **Kevin Gering:** Writing – original draft, Investigation, Formal analysis. **Danielle Henckel:** Writing – original draft, Visualization, Methodology, Investigation, Formal analysis, Data curation. **Andrew Dopilka:** Writing – original draft, Visualization, Investigation, Formal analysis, Data curation. **Nessa Majaya:** Writing – original draft, Visualization, Investigation, Formal analysis. **Robert Kostecki:** Supervision, Methodology, Conceptualization. **Kristin Persson:** Supervision, Methodology. **Gabriel M. Veith:** Writing – review & editing. **Andrew M. Colclasure:** Writing – review & editing, Supervision, Funding acquisition, Conceptualization. **Maxwell C. Schulze:** Writing – review & editing, Writing – original draft, Supervision, Methodology, Funding acquisition, Conceptualization.

Declaration of competing interest

The authors declare that they have no known competing financial interests or personal relationships that could have appeared to influence the work reported in this paper.

Acknowledgments

This work was authored in part by the National Laboratory of the Rockies, operated by Alliance for Energy Innovation, LLC, for the U.S. Department of Energy (DOE) under Contract No. DE-AC36-08GO28308. This work was authored in part by the Idaho National Laboratory, operated by Battelle Energy Alliance, LLC, for the U.S. DOE under Contract No. DE-AC07-05ID14517. This research was supported by the U. S. Department of Energy, Transportation Technologies Office (DOE-TTO) under the Silicon Consortium Project Dive Project, directed by Nicolas Eidson, Carine Steinway, Thomas Do, and Brian Cunningham, and managed by Anthony Burrell. This research used resources of the Advanced Light Source from beamline 2.4, which is a DOE Office of Science User Facility under contract no. DE-AC02-05CH11231. We acknowledge Stephanie Gilbert Corder and Hans Bechtel for aiding in the collection of the SINS spectra at beamline 2.4. We acknowledge Berkeley Marvell NanoLab at CITRIS for providing access to the sputtering and thermal evaporation tool used to fabricate the electrodes in this work. The views expressed in the article do not necessarily represent the views of the DOE or the U.S. Government. The U.S. Government retains and the publisher, by accepting the article for publication, acknowledges that the U.S. Government retains a nonexclusive, paid-up, irrevocable, worldwide license to publish or reproduce the published form of this work, or allow others to do so, for U.S. Government purposes.

Appendix A. Supplementary data

Supplementary material related to this article can be found online at https://doi.org/10.1016/j.est.2026.122559.

Data availability

The data that has been used is confidential.

References

[1] Taeho Yoon, Cao Cuong Nguyen, Daniel M. Seo, Brett L. Lucht, Capacity fading mechanisms of silicon nanoparticle negative electrodes for lithium ion batteries, J. Electrochem. Soc. 162 (12) (2015) A2325, Publisher: IOP Publishing.

[2] Linghong Zhang, Yan Qin, Yuzi Liu, Qi Liu, Yang Ren, Andrew N. Jansen, Wenquan Lu, Capacity fading mechanism and improvement of cycling stability of the SiO anode for lithium-ion batteries, J. Electrochem. Soc. 165 (10) (2018) A2102, Publisher: IOP Publishing.

[3] Wenquan Lu, Linghong Zhang, Yan Qin, Andrew Jansen, Calendar and cycle life of lithium-ion batteries containing silicon monoxide anode, J. Electrochem. Soc. 165 (10) (2018) A2179, Publisher: IOP Publishing.

[4] Javier Bareño, Ilya A. Shkrob, James A. Gilbert, Matilda Klett, Daniel P. Abraham, Capacity fade and its mitigation in Li-ion cells with silicon-graphite electrodes, J. Phys. Chem. C 121 (38) (2017) 20640–20649, Publisher:American Chemical Society.

[5] Harika Dasari, Eric Eisenbraun, Predicting capacity fade in silicon anode-based Li-ion batteries, Energies 14 (5) (2021) 1448, Number: 5 Publisher: Multidisciplinary Digital Publishing Institute.

[6] Josefine D. McBrayer, Marco-Tulio F. Rodrigues, Maxwell C. Schulze, P. Abraham Daniel, A. Apblett Christopher, Ira Bloom, Gerard Michael Carroll, M. Colclasure Andrew, Chen Fang, L. Harrison Katharine, Gao Liu, D. Minteer Shelley, R. Neale Nathan, M. Veith Gabriel, S. Johnson Christopher, T. Vaughey John, K. Burrell Anthony, Brian Cunningham, Calendar aging of silicon-containing batteries, Nat. Energy 6 (9) (2021) 866–872, Number: 9 Publisher: Nature Publishing Group.

[7] Yeyoung Ha, Caleb Stetson, Steven P. Harvey, Glenn Teeter, Bertrand J. Tremolet de Villers, Chun-Sheng Jiang, Manuel Schnabel, Paul Stradins, Anthony Burrell, Sang-Don Han, Effect of water concentration in LiPF6-based electrolytes on the formation, evolution, and properties of the solid electrolyte interphase on Si anodes, ACS Appl. Mater. Interfaces 12 (44) (2020) 49563–49573, Publisher: American Chemical Society.

[8] Hui Yang, Guorong V. Zhuang, Philip N. Ross, Thermal stability of LiPF6 salt and Li-ion battery electrolytes containing LiPF6, J. Power Sources 161 (1) (2006) 573–579.

[9] Ji Yun Han, Seungho Jung, Thermal stability and the effect of water on hydrogen fluoride generation in lithium-ion battery electrolytes containing LiPF6, Batteries 8 (7) (2022) 61, Number: 7 Publisher: Multidisciplinary Digital Publishing Institute.

[10] Mingzhu Liu, Jenel Vatamanu, Xinli Chen, Lidan Xing, Kang Xu, Weishan Li, Hydrolysis of LiPF6-containing electrolyte at high voltage, ACS Energy Lett. 6 (6) (2021) 2096–2102, Publisher: American Chemical Society.

[11] Zhaojuan Li, Fei Xu, Chunlei Li, Peng Wang, Wentao Yi, Shengxian Wang, Li Yang, Chunyan Yan, Shiyou Li, Influences and mechanisms of water on a solid electrolyte interphase film for lithium-ion batteries, ACS Appl Energy Mater. 4 (2) (2021) 1199–1207, Publisher: American Chemical Society.

[12] Janik Lüchtefeld, Hendrik Hemmelmann, Susanne Wachs, J. Mayrhofer Karl, T. Elm Matthias, Balázs B. Berkes, Effect of water contamination on the transition metal dissolution in water-enriched electrolyte: A mechanistic insight into a new type of dissolution, J. Phys. Chem. C 126 (40) (2022) 17204–17211, Publisher: American Chemical Society.

[13] Milena Martins, Dominik Haering, Justin G. Connell, Hao Wan, Katrine L. Svane, Bostjan Genorio, Pedro Farinazzo Bergamo Dias Martins, Pietro P. Lopes, Brian Gould, Filippo Maglia, Roland Jung, Vojislav Stamenkovic, Ivano E. Castelli, Nenad M. Markovic, Jan Rossmeisl, Dusan Strmcnik, Role of catalytic conversions of ethylene carbonate, water, and HF in forming the solid-electrolyte interphase of Li-ion batteries, ACS Catal. 13 (13) (2023) 9289–9301, Publisher: American Chemical Society.

[14] Michael Stich, Nisrit Pandey, Andreas Bund, Drying and moisture resorption behaviour of various electrode materials and separators for lithium-ion batteries, J. Power Sources 364 (2017) 84–91.

[15] Liu-Qun Zheng, Shu-Jun Li, Hai-Jun Lin, Yan-Yue Miaoa, Ling Zhu, Zhong-Jun Zhang, Effects of water contamination on the electrical properties of 18650 lithium-ion batteries, Russ. J. Electrochem. 50 (9) (2014) 904–907.

[16] Shabbir Ahmed, Paul A. Nelson, Dennis W. Dees, Study of a dry room in a battery manufacturing plant using a process model, J. Power Sources 326 (2016) 490–497.

[17] Lars Ole Valøen, N. Reimers Jan, Transport properties of LiPF6-based Li-ion battery electrolytes, J. Electrochem. Soc. 152 (5) (2005) A882, Publisher: IOP Publishing.

[18] S. S Zhang, T. R Jow, K Amine, G. L Henriksen, LiPF6–EC–EMC electrolyte for Li-ion battery, J. Power Sources 107 (1) (2002) 18–23.

[19] Bertrand Philippe, Rémi Dedryvère, Mihaela Gorgoi, Håkan Rensmo, Danielle Gonbeau, Kristina Edström, Role of the LiPF6 salt for the long-term stability of silicon electrodes in Li-ion batteries – a photoelectron spectroscopy study, Chem. Mater. 25 (3) (2013) 394–404, Publisher: American Chemical Society.

[20] Gerardine G. Botte, Ralph E. White, Zhengming Zhang, Thermal stability of LiPF6–EC:EMC electrolyte for lithium ion batteries, J. Power Sources (2001) 97–98, 570–575.

[21] David Yaohui Wang, J.C. Burns, J.R. Dahn, A systematic study of the concentration of lithium hexafluorophosphate (LiPF6) as a salt for LiCoO2/graphite pouch cells, J. Electrochem. Soc. 161 (9) (2014) A1278, Publisher: IOP Publishing.

[22] David Yaohui Wang, N.N. Sinha, R. Petibon, J.C. Burns, J.R. Dahn, A systematic study of well-known electrolyte additives in LiCoO2/graphite pouch cells, J. Power Sources 251 (2014) 311–318.

[23] Sheng Shui Zhang, A review on electrolyte additives for lithium-ion batteries, J. Power Sources 162 (2) (2006) 1379–1394.

[24] Kang Xu, Nonaqueous liquid electrolytes for lithium-based rechargeable batteries, Chem. Rev. 104 (10) (2004) 4303–4418, Publisher: American Chemical Society.

[25] J.C. Burns, N.N. Sinha, Gaurav Jain, Hui Ye, M. VanElzen Collette, Erik Scott, A. Xiao, W.M. Lamanna, J.R. Dahn, The impact of intentionally added water to the electrolyte of Li-ion cells: I. cells with graphite negative electrodes, J. Electrochem. Soc. 160 (11) (2013) A2281, Publisher: IOP Publishing.

[26] J.C. Burns, N.N. Sinha, Gaurav Jain, Hui Ye, M. VanElzen Collette, Erik Scott, A. Xiao, W.M. Lamanna, J.R. Dahn, The impact of intentionally added water to the electrolyte of Li-ion cells: II. cells with lithium titanate negative electrodes, J. Electrochem. Soc. 161 (3) (2013) A247, Publisher: IOP Publishing.

[27] U Langklotz, M. Schneider, A. Michaelis, Water uptake of tape-cast cathodes for lithium ion batteries, J. Ceram. Sci. Technol. (2013).

[28] Wan Liu, Hongwei Cai, Dan Liu, Ruiqing Hua, Hongyang Gao, Ruiming Zhang, Haolin Tang, Junsheng Li, Deyu Qu, The impact of a trace amount of water in an electrolyte on the performance of Li-ion batteries—an empirical kinetic model approach, Int. J. Energy Res. 46 (6) (2022) 7988–7995.

[29] Binayak Roy, Pavel Cherepanov, Cuong Nguyen, Craig Forsyth, Urbi Pal, Tiago Correia Mendes, Patrick Howlett, Maria Forsyth, Douglas MacFarlane, Mega Kar, Lithium borate ester salts for electrolyte application in next-generation high voltage lithium batteries, Adv. Energy Mater. 11 (36) (2021) 2101422.

[30] Shouquan Zhou, Siyu Zhang, Shang Wang, Weiling Zhang, Yan Liu, Hui Lin, Jingjing Chen, Longfei Yan, Fuweng Zhang, Haohong Li, Huidong Zheng, Direct evidences for bis(fluorosulfonyl)imide anion hydrolysis in industrial production: Pathways based on thermodynamics analysis and theoretical simulation, J. Power Sources 577 (2023) 233249.

[31] Evan Walter Clark Spotte-Smith, Thea Bee Petrocelli, Hetal D. Patel, Samuel M. Blau, Kristin A. Persson, Elementary decomposition mechanisms of lithium hexafluorophosphate in battery electrolytes and interphases, ACS Energy Lett. 8 (1) (2023) 347–355, Publisher: American Chemical Society.

[32] Paul G. Kitz, Petr Novák, Erik J. Berg, Influence of water contamination on the SEI formation in Li-ion cells: An operando EQCM-d study, ACS Appl. Mater. Interfaces 12 (13) (2020) 15934–15942, Publisher: American Chemical Society.

[33] Seong Jin An, Jianlin Li, Claus Daniel, Debasish Mohanty, Shrikant Nagpure, David L. Wood, The state of understanding of the lithium-ion-battery graphite solid electrolyte interphase (SEI) and its relationship to formation cycling, Carbon 105 (2016) 52–76.

[34] A.M. Andersson, K. Edström, Chemical composition and morphology of the elevated temperature SEI on graphite, J. Electrochem. Soc. 148 (10) (2001) A1100, Publisher: IOP Publishing.

[35] Julibeth M. Martinez de la Hoz, A. Soto Fernando, Perla B. Balbuena, Effect of the electrolyte composition on SEI reactions at Si anodes of Li-ion batteries, J. Phys. Chem. C 119 (13) (2015) 7060–7068, Publisher: American Chemical Society.

[36] Maxwell C. Schulze, Fernando Urias, Nikita S. Dutta, Zoey Huey, Jaclyn Coyle, Glenn Teeter, Ryan Doeren, Bertrand J. Tremolet de Villers, Sang-Don Han, Nathan R. Neale, G. Michael Carroll, Control of nanoparticle dispersion, SEI composition, and electrode morphology enables long cycle life in high silicon content nanoparticle-based composite anodes for lithium-ion batteries, J. Mater. Chem. A 11 (10) (2023) 5257–5266, Publisher: Royal Society of Chemistry.

[37] Gabriel M. Veith, Mathieu Doucet, J. Kevin Baldwin, L. Sacci Robert, M. Fears Tyler, Yongqiang Wang, James F. Browning, Direct determination of solid-electrolyte interphase thickness and composition as a function of state of charge on a silicon anode, J. Phys. Chem. C 119 (35) (2015) 20339–20349, Publisher: American Chemical Society.

[38] Mengyun Nie, P. Abraham Daniel, Yanjing Chen, Arijit Bose, Brett L. Lucht, Silicon solid electrolyte interphase (SEI,) of lithium ion battery characterized by microscopy and spectroscopy, J. Phys. Chem. C 117 (26) (2013) 13403–13412, Publisher:American Chemical Society.

[39] Nyr E. Galushkin, N.N. Yazvinskaya, D.N. Galushkin, Mechanism of gases generation during lithium-ion batteries cycling, J. Electrochem. Soc. 166 (6) (2019) A897–A908.

[40] Stefan Ilic, Milena Martins, Haoyu Liu, Pedro Farinazzo Bergamo Dias Martins, Dominik Haering, Jingtian Yang, Toru Hatsukade, Bostjan Genorio, Stephen E. Weitzner, Liwen F. Wan, Zhengcheng Zhang, Justin G. Connell, Baris Key, Jordi Cabana, Dusan Strmcnik, An unwanted guest in the electrochemical oxidation of high-voltage li-ion battery electrolytes: the life of highly reactive protons, Energy Environ. Sci. (2025) Publisher: Royal Society of Chemistry.

[41] Rui Guo, M. Gallant Betar, Li2o solid electrolyte interphase: Probing transport properties at the chemical potential of lithium, Chem. Mater. 32 (13) (2020) 5525–5533, Publisher: American Chemical Society.

[42] Xinyang Chen, Ming Jiang, Xinyu Du, Xuejie Gao, Kun Feng, Yulong Liu, Xiaofei Yang, Runcang Sun, Dan Luo, Zhongwei Chen, Li2O-enhanced solid electrolyte interphase surpassing lif-only sei for high-performance all-solid-state li batteries, Adv. Energy Mater. (2025) 2502589.

[43] Shufen Wu, Nian Zhang, Jintao Du, Feifan Tao, Wenjun Ma, Xinyuan Yin, Yibo Wang, Hui Zhang, Pengfei Yu, Xuefei Feng, et al., A multifunctional molecular modulated strategy featuring novel Li+ transport centers and Li2O-rich SEI layer for high-performance all-solid-state lithium metal batteries, Angew. Chem. Int. Ed. 64 (20) (2025) e202422942.

[44] R.B. Derr, C.B. Willmore, Dehydration of organic liquids with activated alumina, Ind. Eng. Chem. 31 (7) (1939) 866–868, Publisher: American Chemical Society (ACS).

[45] D.W. Breck, J.V. Smith, Molecular sieves, Sci. Am. 200 (1) (1959) 85–96, Publisher: Scientific American, a division of Nature America, Inc.

[46] Ye Shui Zhang, Nicola E. Courtier, Zhenyu Zhang, Kailong Liu, Josh J. Bailey, Adam M. Boyce, Giles Richardson, Paul R. Shearing, Emma Kendrick, Dan J.L. Brett, A review of lithium-ion battery electrode drying: mechanisms and metrology, Adv. Energy Mater. 12 (2) (2022) 2102233.

[47] Zhi Chang, Yu Qiao, Han Deng, Huijun Yang, Ping He, Haoshen Zhou, A stable high-voltage lithium-ion battery realized by an in-built water scavenger, Energy Environ. Sci. 13 (4) (2020) 1197–1204, Publisher: Chemis: Royal Society of Chemistry.

[48] Jung-Gu Han, Koeun Kim, Yongwon Lee, Nam-Soon Choi, Scavenging materials to stabilize LiPF6-containing carbonate-based electrolytes for Li-ion batteries, Adv. Mater. 31 (20) (2019) 1804822.

[49] Jung-Gu Han, Chihyun Hwang, Su Hwan Kim, Chanhyun Park, Jonghak Kim, Gwan Yeong Jung, Kyungeun Baek, Sujong Chae, Seok Ju Kang, Jaephil Cho, et al., An antiaging electrolyte additive for high-energy-density lithium-ion batteries, Adv. Energy Mater. 10 (20) (2020) 2000563.
[50] Drew J. Pereira, Hunter A. McRay, Saurabh S. Bopte, Golareh Jalilvand, H2O/HF scavenging mechanism in cellulose-based separators for lithium-ion batteries with enhanced cycle life, ACS Appl. Mater. Interfaces 16 (5) (2024) 5745–5757, Publisher: American Chemical Society.
[51] Xia Cao, Hao Jia, Wu Xu, Ji-Guang Zhang, Review—localized high-concentration electrolytes for lithium batteries, J. Electrochem. Soc. 168 (1) (2021) 010522, Publisher: IOP Publishing.
[52] Shuru Chen, Jianming Zheng, Lu Yu, Xiaodi Ren, Mark H. Engelhard, Chaojiang Niu, Hongkyung Lee, Wu Xu, Jie Xiao, Jun Liu, et al., High-efficiency lithium metal batteries with fire-retardant electrolytes, Joule 2 (8) (2018) 1548–1558.
[53] Xiaodi Ren, Peiyuan Gao, Lianfeng Zou, Shuhong Jiao, Xia Cao, Xianhui Zhang, Hao Jia, Mark H. Engelhard, Bethany E. Matthews, Haiping Wu, et al., Role of inner solvation sheath within salt–solvent complexes in tailoring electrode/electrolyte interphases for lithium metal batteries, Proc. Natl. Acad. Sci. 117 (46) (2020) 28603–28613.
[54] Helen K. Bergstrom, Bryan D. McCloskey, Ion transport in (localized) high concentration electrolytes for Li-based batteries, ACS Energy Lett. 9 (2) (2024) 373–380, Publisher:American Chemical Society.
[55] Taku Sudoh, Shuhei Ikeda, Keisuke Shigenobu, Seiji Tsuzuki, Kaoru Dokko, Masayoshi Watanabe, Wataru Shinoda, Kazuhide Ueno, Li-ion transport and solution structure in sulfolane-based localized high-concentration electrolytes, J. Phys. Chem. C 127 (25) (2023) 12295–12303, Publisher: American Chemical Society.
[56] Yanzhou Wu, Aiping Wang, Qiao Hu, Hongmei Liang, Hong Xu, Li Wang, Xiangming He, Significance of antisolvents on solvation structures enhancing interfacial chemistry in localized high-concentration electrolytes, J. ACS Central Sci. 8 (9) (2022) 1290–1298, Publisher: American Chemical Society.
[57] Yanzhou Wu, Pengyun Yu, TianTian Dong, Li Wang, Hong Xu, Jianping Wang, Xiangming He, Unraveling the molecular mechanisms of antisolvent action in localized high-concentration electrolytes for lithium metal batteries, Mater. Today 83 (2025) 223–230.
[58] Wessel van Ekeren, Aram Hall, Katja Lahtinen, Reza Younesi, The solvation structure of localized high concentration electrolytes, ChemElectroChem 11 (11) (2024) e202400050.
[59] Yu Zheng, A. Soto Fernando, Victor Ponce, Jorge M. Seminario, Xia Cao, Ji-Guang Zhang, Perla B. Balbuena, Localized high concentration electrolyte behavior near a lithium–metal anode surface, J. Mater. Chem. A 7 (43) (2019) 25047–25055, Publisher: The Royal Society of Chemistry.
[60] Ye Xiao, Rui Xu, Lei Xu, Jun-Fan Ding, Jia-Qi Huang, Recent advances in anion-derived SEIs for fast-charging and stable lithium batteries, Energy Mater. 1 (2) (2021) N/A–N/A, Publisher: OAE Publishing Inc.
[61] Feng Guo, Xi Chen, Yuhan Hou, Wenshuo Wei, Zhicheng Wang, Hao Yu, Jingjing Xu, Improved cycling of Li|| NMC811 batteries under practical conditions by a localized high-concentration electrolyte, Small 19 (16) (2023) 2207290.
[62] Bikila Nagasa Olana, D. Lin Shawn, Bing-Joe Hwang, *In situ* diffuse reflectance infrared fourier-transformed spectroscopy study of solid electrolyte interphase formation from lithium bis(trifluoromethanesulfonyl)imide in 1, 2-dimethoxyethane and 1, 3-dioxolane with and without lithium nitrate additive over lithium and copper metal anodes, Electrochim. Acta 416 (2022) 140266.
[63] Daniel M. Seo, Stefanie Reininger, Mary Kutcher, Kaitlin Redmond, B. Euler William, Brett L. Lucht, Role of mixed solvation and ion pairing in the solution structure of lithium ion battery electrolytes, J. Phys. Chem. C 119 (25) (2015) 14038–14046, Publisher: American Chemical Society.
[64] Tianyang Wang, Ruichen Wan, Zhenghuan Tang, Jun Wei Yap, Jieren Shao, Lei Qin, Songwei Zhang, Junbin Choi, Yiying Wu, Jung-Hyun Kim, Dual-salts localized high-concentration electrolyte for Li-and Mn-rich high-voltage cathodes in lithium metal batteries, Small 20 (42) (2024) 2401364.
[65] Hanlu Zheng, Yu Zhong, Changdong Gu, Xiuli Wang, Jiangping Tu, Anion-derived solid electrolyte interphase enabled by diluent modulated dimethyl carbonate-based localized high concentration electrolytes for lithium metal batteries, Batter. Supercaps 7 (11) (2024) e202400238.
[66] Li-Li Jiang, Chong Yan, Yu-Xing Yao, Wenlong Cai, Jia-Qi Huang, Qiang Zhang, Inhibiting solvent co-intercalation in a graphite anode by a localized high-concentration electrolyte in fast-charging batteries, Angew. Chem. Int. Ed. 60 (7) (2021) 3402–3406.
[67] Seho Sun, Gaeun Kim, Dongsoo Lee, Eunkyung Park, Seungcheol Myeong, Byoungkuk Son, Kangchun Lee, Minchul Jang, Ungyu Paik, Taeseup Song, Modulating SEI formation via tuning the solvation sheath for lithium metal batteries, Chem. Commun. 58 (70) (2022) 9834–9837.
[68] Yanli Yin, Elisabetta Arca, Luning Wang, Guang Yang, Manuel Schnabel, Lei Cao, Chuanxiao Xiao, Hongyao Zhou, Ping Liu, Jagjit Nanda, et al., Nonpassivated silicon anode surface, ACS Appl. Mater. Interfaces 12 (23) (2020) 26593–26600.
[69] Evelyna Wang, Marco-Tulio Fonseca Rodrigues, Baris Key, Quantifying the reactivity of isolated Li x Si domains in Si anodes using operando NMR, J. Phys. Chem. Lett. 16 (2025) 12290–12297.
[70] Minseong Ko, Sujong Chae, Jaephil Cho, Challenges in accommodating volume change of Si anodes for Li-ion batteries, ChemElectroChem 2 (11) (2015) 1645–1651.
[71] Chunlei Li, Yu Zhu, Yin Quan, Feifei Zong, Jie Wang, Dongni Zhao, Ningshuang Zhang, Peng Wang, Xiaoling Cui, Shiyou Li, Mitigating volume expansion of silicon-based anode through interfacial engineering based on intermittent discharge strategy, J. Energy Chem. 98 (2024) 680–691.
[72] Ju-Myung Kim, Ran Yi, Xia Caoand, Yaobin Xu, Mark Engelhard, Shalini Tripathi, Chongmin Wang, Ji-Guang Zhang, Extending calendar life of Si-based lithium-ion batteries by a localized high concentration electrolyte, ACS Energy Lett. 9 (5) (2024) 2318–2325, Publisher: American Chemical Society.
[73] Maxwell C. Schulze, Nina Prakash, Kevin Gering, M. Colclasure Andrew, Peter J. Weddle, Predicting Si-anode calendar life using machine learning: Correlating electrolyte properties and electrochemical signals, J. Power Sources 659 (2025) 238338.
[74] Hong-Bo Han, Si-Si Zhou, Dai-Jun Zhang, Shao-Wei Feng, Li-Fei Li, Kai Liu, Wen-Fang Feng, Jin Nie, Hong Li, Xue-Jie Huang, et al., Lithium bis (fluorosulfonyl) imide (LiFSI) as conducting salt for nonaqueous liquid electrolytes for lithium-ion batteries: Physicochemical and electrochemical properties, J. Power Sources 196 (7) (2011) 3623–3632.
[75] David Reber, Renato Figi, Ruben-Simon Kühnel, Corsin Battaglia, Stability of aqueous electrolytes based on LiFSI and NaFSI, Electrochim. Acta 321 (2019) 134644.
[76] Corey M. Efaw, Qisheng Wu, Ningshengjie Gao, Yugang Zhang, Haoyu Zhu, Kevin Gering, Michael F. Hurley, Hui Xiong, Enyuan Hu, Xia Cao, et al., Localized high-concentration electrolytes get more localized through micelle-like structures, Nat. Mater. 22 (12) (2023) 1531–1539.
[77] Juliane I. Preimesberger, L.E. Usseglio-Viretta Francois, Ankit Verma, Avtar Singh, M. Colclasure Andrew, Patrick Walker, Glenn Teeter, F. Pach Gregory, John Westgard, Fernando Urias-Cordero, R. Neale Nathan, E. Coyle Jaclyn, G. Michael Carroll, The effect of nanoparticle size on calendar and cycle lifetimes of silicon anode lithium-ion batteries, EES Batter. 1 (2) (2025) 298–309, Publisher: Royal Society of Chemistry.
[78] Maxwell C. Schulze, Gerard Michael Carroll, Trevor R. Martin, Kevin Sanchez-Rivera, Fernando Urias, Nathan R. Neale, Hydrophobic versus hydrophilic interfacial coatings on silicon nanoparticles teach us how to design the solid electrolyte interphase in silicon-based Li-ion battery anodes, ACS Applied Energy Materials 4 (2) (2021) 1628–1636, Publisher: American Chemical Society.
[79] Lance M. Wheeler, C. Anderson Nicholas, K.B. Palomaki Peter, L. Blackburn Jeffrey, C. Johnson Justin, Nathan R. Neale, Silyl radical abstraction in the functionalization of plasma-synthesized silicon nanocrystals, Chem. Mater. 27 (19) (2015) 6869–6878, Publisher: American Chemical Society.
[80] Marco-Tulio F. Rodrigues, Addressing limitations of the endpoint slippage analysis, J. Electrochem. Soc. 171 (12) (2024) 120535, Publisher: IOP Publishing.
[81] United States advanced battery consortium battery test manual for electric vehicles, 2020.
[82] M.J. Piernas-Muñoz, S.E. Trask, A.R. Dunlop, E. Lee, I. Bloom, Effect of temperature on silicon-based anodes for lithium-ion batteries, J. Power Sources 441 (2019) 227080.
[83] Grietus Mulder, Noshin Omar, Stijn Pauwels, Filip Leemans, Bavo Verbrugge, Wouter De Nijs, Peter Van den Bossche, Daan Six, Joeri Van Mierlo, Enhanced test methods to characterise automotive battery cells, J. Power Sources 196 (23) (2011) 10079–10087.
[84] Zachary Ruff, Chao Xu, Clare P Grey, Transition metal dissolution and degradation in NMC811-graphite electrochemical cells, J. Electrochem. Soc. 168 (6) (2021) 060518.
[85] Roland Jung, Fabian Linsenmann, Rowena Thomas, Johannes Wandt, Sophie Solchenbach, Filippo Maglia, Christoph Stinner, Moniek Tromp, Hubert A. Gasteiger, Nickel and manganese, and cobalt dissolution from Ni-rich NMC and their effects on NMC622-graphite cells, J. Electrochem. Soc. 166 (2) (2019) A378–A389.
[86] David Nečas, Petr Klapetek, Gwyddion: an open-source software for SPM data analysis, Open Phys. 10 (1) (2012) 181–188, Publisher: De Gruyter Open Access.
[87] Jonathan M. Larson, Hans A. Bechtel, Robert Kostecki, Detection and signal processing for near-field nanoscale fourier transform infrared spectroscopy, Adv. Funct. Mater. 34 (46) (2024) 2406643.
[88] Kevin L. Gering, Computer Model for Characterizing, Screening, and Optimizing Electrolyte Systems, Technical report, Idaho National Laboratory (INL), Idaho Falls, ID (United States), 2015.
[89] Evgeny Epifanovsky, T.B. Gilbert Andrew, Xintian Feng, Joonho Lee, Yuezhi Mao, Narbe Mardirossian, Pavel Pokhilko, F. White Alec, P. Coons Marc, L. Dempwolff Adrian, Zhengting Gan, Diptarka Hait, R. Horn Paul, D. Jacobson Leif, Ilya Kaliman, Jörg Kussmann, W. Lange Adrian, Ka Un Lao, S. Levine Daniel, Jie Liu, C. McKenzie Simon, Adrian F. Morrison, D. Nanda Kaushik, Felix Plasser, R. Rehn Dirk, L. Vidal Marta, Zhi-Qiang You, Ying Zhu, Bushra Alam, J. Albrecht Benjamin, Abdulrahman Aldossary, Ethan Alguire, H. Andersen Josefine, Vishikh Athavale, Dennis Barton, Khadiza Begam, Andrew Behn,

Nicole Bellonzi, A. Bernard Yves, J. Berquist Eric, G.A. Burton Hugh, Abel Carreras, Kevin Carter-Fenk, Romit Chakraborty, D. Chien Alan, D. Closser Kristina, Vale Cofer-Shabica, Saswata Dasgupta, Marc de Wergifosse, Jia Deng, Michael Diedenhofen, Hainam Do, Sebastian Ehlert, Po-Tung Fang, Shervin Fatehi, Qingguo Feng, Triet Friedhoff, James Gayvert, Qinghui Ge, Gergely Gidofalvi, Matthew Goldey, Joe Gomes, E. González-Espinoza Cristina, Sahil Gulania, O. Gunina Anastasia, W.D. Hanson-Heine Magnus, H.P. Harbach Phillip, Andreas Hauser, F. Herbst Michael, Mario Hernández Vera, Manuel Hodecker, C. Holden Zachary, Shannon Houck, Xunkun Huang, Kerwin Hui, C. Huynh Bang, Maxim Ivanov, Ádám Jász, Hyunjun Ji, Hanjie Jiang, Benjamin Kaduk, K.ähler Sven, Kirill Khistyaev, Jaehoon Kim, Gergely Kis, Phil Klunzinger, Zsuzsanna Koczor-Benda, Joong Hoon Koh, Dimitri Kosenkov, Laura Koulias, Tim Kowalczyk, M. Krauter Caroline, Karl Kue, Alexander Kunitsa, Thomas Kus, István Ladjánszki, Arie Landau, V. Lawler Keith, Daniel Lefrancois, Susi Lehtola, R. Li Run, Yi-Pei Li, Jiashu Liang, Marcus Liebenthal, Hung-Hsuan Lin, You-Sheng Lin, Fenglai Liu, Kuan-Yu Liu, Matthias Loipersberger, Arne Luenser, Aaditya Manjanath, Prashant Manohar, Erum Mansoor, F. Manzer Sam, Shan-Ping Mao, V. Marenich Aleksandr, Thomas Markovich, Stephen Mason, A. Maurer Simon, F. McLaughlin Peter, Maximilian F.S.J. Menger, Jan-Michael Mewes, A. Mewes Stefanie, Pierpaolo Morgante, J. Wayne Mullinax, J. Oosterbaan Katherine, Garrette Paran, C. Paul Alexander, K. Paul Suranjan, Fabijan Pavošević, Zheng Pei, Stefan Prager, I. Proynov Emil, Ádám Rák, Eloy Ramos-Cordoba, Bhaskar Rana, E. Rask Alan, Adam Rettig, M. Richard Ryan, Fazle Rob, Elliot Rossomme, Tarek Scheele, Maximilian Scheurer, Matthias Schneider, Nickolai Sergueev, M. Sharada Shaama, Wojciech Skomorowski, W. Small David, J. Stein Christopher, Yu-Chuan Su, J. Sundstrom Eric, Zhen Tao, Jonathan Thirman, Gábor J. Tornai, Takashi Tsuchimochi, M. Tubman Norm, Srimukh Prasad Veccham, Oleg Vydrov, Jan Wenzel, Jon Witte, Atsushi Yamada, Kun Yao, Sina Yeganeh, R. Yost Shane, Alexander Zech, Igor Ying Zhang, Xing Zhang, Yu Zhang, Dmitry Zuev, Alán Aspuru-Guzik, T. Bell Alexis, A. Besley Nicholas, B. Bravaya Ksenia, R. Brooks Bernard, David Casanova, Jeng-Da Chai, Sonia Coriani, J. Cramer Christopher, György Cserey, A. Eugene DePrince III, Robert A. DiStasio Jr., Andreas Dreuw, D. Dunietz Barry, R. Furlani Thomas, A. Goddard III William, Sharon Hammes-Schiffer, Teresa Head-Gordon, J. Hehre Warren, Chao-Ping Hsu, Thomas-C. Jagau, Yousung Jung, Andreas Klamt, Jing Kong, S. Lambrecht Daniel, WanZhen Liang, J. Mayhall Nicholas, C. William McCurdy, Jeffrey B. Neaton, Christian Ochsenfeld, A. Parkhill John, Roberto Peverati, A. Rassolov Vitaly, Yihan Shao, V. Slipchenko Lyudmila, Tim Stauch, P. Steele Ryan, E. Subotnik Joseph, J.W. Thom Alex, Alexandre Tkatchenko, G. Truhlar Donald, Troy Van Voorhis, A. Wesolowski Tomasz, K. Birgitta Whaley, H. Lee Woodcock, Paul M. Zimmerman III, Shirin Faraji, M.W. Gill Peter, Martin Head-Gordon, M. Herbert John, Anna I. Krylov, Software for the frontiers of quantum chemistry: An overview of developments in the q-chem 5 package, J. Chem. Phys. 155 (8) (2021) 084801.

[90] Peter Eastman, Raimondas Galvelis, Raúl P. Peláez, Charlles R.A. Abreu, E. Farr Stephen, Emilio Gallicchio, Anton Gorenko, M. Henry Michael, Frank Hu, Jing Huang, Andreas Krämer, Julien Michel, A. Mitchell Joshua, S. Pande Vijay, João PGLM Rodrigues, Jaime Rodriguez-Guerra, C. Simmonett Andrew, Sukrit Singh, Jason Swails, Philip Turner, Yuanqing Wang, Ivy Zhang, D. Chodera John, Gianni De Fabritiis, Thomas E. Markland, OpenMM 8: Molecular dynamics simulation with machine learning potentials, J. Phys. Chem. B 128 (1) (2024) 109–116, Publisher: American Chemical Society.

[91] Alex M. Ganose, Hrushikesh Sahasrabuddhe, Mark Asta, Kevin Beck, Tathagata Biswas, Alexander Bonkowski, Joana Bustamante, Xin Chen, Yuan Chiang, Daryl C. Chrzan, Jacob Clary, Orion A. Cohen, Christina Ertural, Max C. Gallant, Janine George, Sophie Gerits, Rhys E.A. Goodall, Rishabh D. Guha, Geoffroy Hautier, Matthew Horton, T.J. Inizan, Aaron D. Kaplan, Ryan S. Kingsbury, Matthew C. Kuner, Bryant Li, Xavier Linn, Matthew J. McDermott, Rohith Srinivaas Mohanakrishnan, Aakash N. Naik, Jeffrey B. Neaton, Shehan M. Parmar, Kristin A. Persson, Guido Petretto, Thomas A.R. Purcell, Francesco Ricci, Benjamin Rich, Janosh Riebesell, Gian-Marco Rignanese, Andrew S. Rosen, Matthias Scheffler, Jonathan Schmidt, Jimmy-Xuan Shen, Andrei Sobolev, Ravishankar Sundararaman, Cooper Tezak, Victor Trinquet, Joel B. Varley, Derek Vigil-Fowler, Duo Wang, David Waroquiers, Mingjian Wen, Han Yang, Hui Zheng, Jiongzhi Zheng, Zhuoying Zhu, Anubhav Jain, Atomate2: Modular workflows for materials science, Digit. Discov. (2025).

[92] Leandro Martínez, Ricardo Andrade, Ernesto G. Birgin, José Mario Martínez, Packmol: A package for building initial configurations for molecular dynamics simulations, J. Comput. Chem. 30 (13) (2009) 2157–2164.

[93] Simon Boothroyd, Pavan Kumar Behara, Owen C. Madin, David F. Hahn, Hyesu Jang, Vytautas Gapsys, Jeffrey R. Wagner, Joshua T. Horton, David L Dotson, Matthew W. Thompson, et al., Development and benchmarking of open force field 2.0. 0: The sage small molecule force field, J. Chem. Theory and Comput. 19 (11) (2023) 3251–3275.

[94] Igor Leontyev, Alexei Stuchebrukhov, Accounting for electronic polarization in non-polarizable force fields, Phys. Chem. Chem. Phys. 13 (7) (2011) 2613–2626.

[95] Mangesh I. Chaudhari, Jijeesh R. Nair, Lawrence R. Pratt, Fernando A. Soto, Perla B. Balbuena, Susan B. Rempe, Scaling atomic partial charges o.f carbonate solvents for lithium ion solvation and diffusion, J. Chem. Theory Comput. 12 (12) (2016) 5709–5718.

[96] Orion Archer Cohen, Hugo Macdermott-Opeskin, Lauren Lee, Tingzheng Hou, Kara D. Fong, Ryan Kingsbury, Jingyang Wang, Kristin A. Persson, Solvationanalysis: A python toolkit for understanding liquid solvation structure in classical molecular dynamics simulations, J. Open Source Softw. 8 (84) (2023) 5183.

[97] Richard J. Gowers, Max Linke, Jonathan Barnoud, Tyler John Edward Reddy, Manuel N. Melo, Sean L. Seyler, Jan Domanski, David L. Dotson, Sébastien Buchoux, Ian M. Kenney, et al., Mdanalysis: a Python Package for the Rapid Analysis of Molecular Dynamics Simulations, Technical report, Los Alamos National Laboratory (LANL), Los Alamos, NM (United States), 2019.

[98] Marco-Tulio F. Rodrigues, Kaushik Kalaga, E. Trask Stephen, A. Shkrob Ilya, Daniel P. Abraham, Anode-dependent impedance rise in layered-oxide cathodes of lithium-ion cells, J. Electrochem. Soc. 165 (9) (2018) A1697, Publisher: IOP Publishing.

[99] Marco-Tulio F. Rodrigues, Ganguli Babu, Hemtej Gullapalli, Kaushik Kalaga, N. Sayed Farheen, Keiko Kato, Jarin Joyner, Pulickel M. Ajayan, A materials perspective on Li-ion batteries at extreme temperatures, Nat. Energy 2 (8) (2017) 17108, Publisher: Nature Publishing Group.

[100] Guanyao Wang, Qian-Kui Zhang, Xue-Qiang Zhang, Jun Lu, Chengang Pei, Donghyun Min, Jia-Qi Huang, Ho Seok Park, Electrolyte additive for interfacial engineering of lithium and zinc metal anodes, Adv. Energy Mater. 15 (2) (2025) 2304557.

[101] Nam-Soon Choi, Kyoung Han Yew, Kyu Youl Lee, Minseok Sung, Ho Kim, Sung-Soo Kim, Effect of fluoroethylene carbonate additive on interfacial properties of silicon thin-film electrode, J. Power Sources 161 (2) (2006) 1254–1259.

[102] Kiyoshi Kanamura, Soshi Shiraishi, Zen ichiro Takehara, Electrochemical deposition of very smooth lithium using nonaqueous electrolytes containing HF, J. Electrochem. Soc. 143 (7) (1996) 2187, Publisher: IOP Publishing.

[103] Rod McMillan, Helen Slegr, Z.X. Shu, Weidong Wang, Fluoroethylene carbonate electrolyte and its use in lithium ion batteries with graphite anodes, J. Power Sources (1999) 81–82, 20–26.

[104] Borui Yang, Anjun Hu, Ting Li, Kun Li, Yuanjian Li, Jingyun Jiang, Zhubing Xiao, Zhi Wei Seh, Jianping Long, Eliminating water hazards and regulating electrode-electrolyte interfaces by multifunctional sacrificial electrolyte additives for long-life lithium metal batteries, Energy Storage Mater. 70 (2024) 103512.

[105] Liumin Suo, Oleg Borodin, Tao Gao, Marco Olguin, Janet Ho, Xiulin Fan, Chao Luo, Chunsheng Wang, Kang Xu, "Water-in-salt" electrolyte enables high-voltage aqueous lithium-ion chemistries, Science 350 (6263) (2015) 938–943, Publisher: American Association for the Advancement of Science.

[106] Fei Wang, Oleg Borodin, S. Ding Michael, Mallory Gobet, Jenel Vatamanu, Xiulin Fan, Tao Gao, Nico Eidson, Yujia Liang, Wei Sun, Steve Greenbaum, Kang Xu, Chunsheng Wang, Hybrid aqueous/non-aqueous electrolyte for safe and high-energy Li-ion batteries, Joule 2 (5) (2018) 927–937, Publisher: Elsevier.

[107] Guinevere A. Giffin, The role of concentration in electrolyte solutions for non-aqueous lithium-based batteries, Nat. Commun. 13 (1) (2022) 5250, Publisher: Nature Publishing Group.

[108] Dongliang Chao, Shi-Zhang Qiao, Toward high-voltage aqueous batteries: Super- or low-concentrated electrolyte? Joule 4 (9) (2020) 1846–1851, Publisher:Elsevier.

[109] Marco-Tulio F. Rodrigues, Coulombic efficiency and capacity retention are not universal descriptors of cell aging, J. Electrochem. Soc. 169 (11) (2022) 110514, Publisher: IOP Publishing.

[110] Bernardine L.D. Rinkel, David S. Hall, Israel Temprano, Clare P. Grey, Electrolyte oxidation pathways in lithium-ion batteries, J. Am. Chem. Soc. 142 (35) (2020) 15058–15074.

[111] Marco-Tulio F. Rodrigues, Capacity and coulombic efficiency measurements underestimate the rate of SEI growth in silicon anodes, J. Electrochem. Soc. 169 (8) (2022) 080524, Publisher:IOP Publishing.

[112] Peter Keil, Andreas Jossen, Impact of dynamic driving loads and regenerative braking on the aging of lithium-ion batteries in electric vehicles, J. Electrochem. Soc. 164 (13) (2017) A3081, Publisher: IOP Publishing.

[113] A.J. Smith, J.C. Burns, D. Xiong, J.R. Dahn, Interpreting high precision coulometry results on Li-ion cells, J. Electrochem. Soc. 158 (10) (2011) A1136, Publisher: IOP Publishing.

[114] Andrew Dopilka, Jonathan M. Larson, Hyungyeon Cha repory, Robert Kostecki, Synchrotron near-field infrared nanospectroscopy and nanoimaging of lithium fluoride in solid electrolyte interphases in Li-ion battery anodes, ACS Nano 18 (23) (2024) 15270–15283, Publisher: American Chemical Society.

[115] Maxwell C. Schulze, Marco-Tulio F. Rodrigues, D. McBrayer Josefine, P. Abraham Daniel, A. Apblett Christopher, Ira Bloom, Zonghai Chen, M. Colclasure Andrew, R. Dunlop Alison, Chen Fang, L. Harrison Katharine, Gao Liu, D. Minteer Shelley, R. Neale Nathan, David Robertson, P. Tornheim Adam, E. Trask Stephen, M. Veith Gabriel, Ankit Verma, Zhenzhen Yang, Christopher Johnson, Critical evaluation of potentiostatic holds as accelerated predictors of capacity fade during calendar aging, J. Electrochem. Soc. 169 (5) (2022) 050531, Publisher:Capacity Fade during Calendar AgingIOP Publishing.

[116] I. Rey, P. Johansson, J. Lindgren, J.C. Lassègues, J. Grondin, L. Servant, Spectroscopic and theoretical study of (CF3SO2)2N- (TFSI-) and (CF3SO2)2NH (HTFSI), J. Phys. Chem. A 102 (19) (1998) 3249–3258, Publisher: American Chemical Society.

[117] K.C. Schreiber, Infrared spectra of sulfones and related compounds, Anal. Chem. 21 (10) (1949) 1168–1172.

[118] E. Peled, D. Golodnitsky, G. Ardel, Advanced model for solid electrolyte interphase electrodes in liquid and polymer electrolytes, J. Electrochem. Soc. 144 (8) (1997) L208, Publisher: IOP Publishing.

[119] William D. Richards, J. Miara Lincoln, Yan Wang, Jae Chul Kim, Gerbrand Ceder, Interface stability in solid-state batteries, Chem. Mater. 28 (1) (2016) 266–273, Publisher: American Chemical Society.

[120] Simon Lorger, Robert Usiskin, Joachim Maier, Transport and charge carrier chemistry in lithium oxide, J. Electrochem. Soc. 166 (10) (2019) A2215, Publisher: IOP Publishing.

[121] Gustavo M. Hobold, Chongzhen Wang, Katherine Steinberg, Yuzhang Li, Betar M. Gallant, High lithium oxide prevalence in the lithium solid–electrolyte interphase for high coulombic efficiency, Nat. Energy 9 (5) (2024) 580–591, Publisher: Nature Publishing Group.

[122] Graham Leverick, Yang Shao-Horn, Controlling electrolyte properties and redox reactions using solvation and implications in battery functions: a mini-review, Adv. Energy Mater. 13 (13) (2023) 2204094.

[123] Judith Alvarado, A. Schroeder Marshall, Minghao Zhang, Oleg Borodin, Eric Gobrogge, Marco Olguin, S. Ding Michael, Mallory Gobet, Steve Greenbaum, Ying Shirley Meng, Kang Xu, A carbonate-free, sulfone-based electrolyte for high-voltage Li-ion batteries, Mater. Today 21 (4) (2018) 341–353.

[124] Pengcheng Li, Hao Zhang, Jun Lu, Ge Li, Low concentration sulfolane-based electrolyte for high voltage lithium metal batteries, Angew. Chem. 135 (10) (2023) e202216312.

[125] H.-G. Schweiger, Michael Multerer, U. Wietelmann, J.-C. Panitz, T. Burgemeister, Heiner Jakob Gores, Nmr determination of trace water in lithium salts for battery electrolytes, J. Electrochem. Soc. 152 (3) (2005) A622–A627.

[126] Tianshi Lv, Liumin Suo, Water-in-salt widens the electrochemical stability window: Thermodynamic and kinetic factors, Curr. Opin. Electrochem. 29 (2021) 100818.

[127] Yiqing Liao, Huiyan Zhang, Yufan Peng, Yonggang Hu, Jinding Liang, Zhengliang Gong, Yimin Wei, Yong Yang, Electrolyte degradation during aging process of lithium-ion batteries: mechanisms, characterization, and quantitative analysis, Adv. Energy Mater. 14 (18) (2024) 2304295.